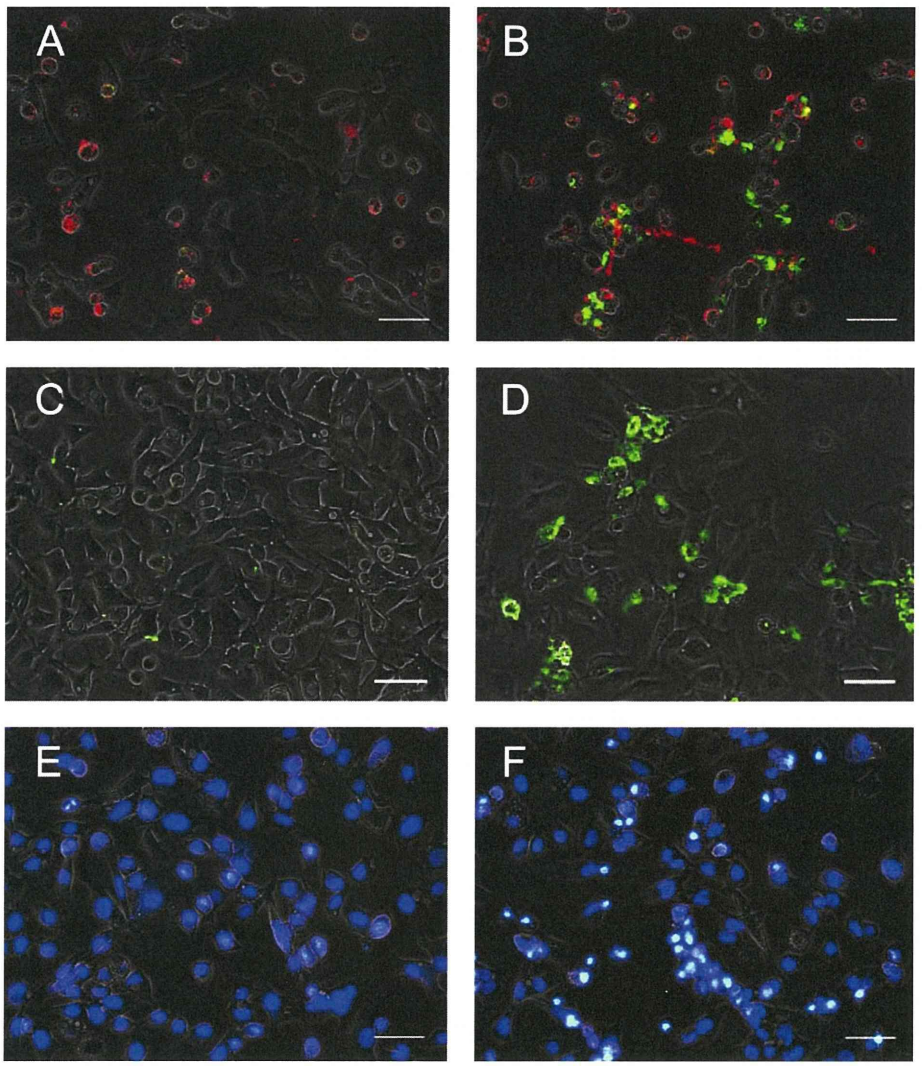

Fig. 6. Fluorescent microscopic images of HepG2 cells at 6 h after TiO_2/US treatment. The HepG2 cells were stained with JC-1 (A and B), Annexin V-FITC (C and D), and DAPI (E and F), respectively. (A, C and E) control condition without treatment, (B, D and F) with TiO_2/US treatment. The fluorescent images were merged with the phase-contrast ones. Each scale bar indicates 50 μm. (For interpretation of the references to colour in this figure legend, the reader is referred to the web version of this article.)

binding to target cells, as reported in the PDT using TiO_2 NPs [17–19]. The present study clarified that it took 6 h for the pre-S1/S2-mediated specific uptake of TiO_2 NPs by HepG2 cells (Fig. 1). This is consistent with the report that the fusion of the hepatitis B virus toward liver cells was complete within 6 h [30].

On the other hand, without pre-S1/S2, our TiO_2 NPs were not incorporated by either the HepG2 or WiDr cells under the examined condition (Fig. 2A and C). There is one report that the TiO_2 NPs used for the PDT was incorporated to glioma cells within 3 h, even without modification by any targeting biomolecules [15]. In general, the TiO_2 NPs which exhibit nonspecific incorporation cannot be used as a practical sonosensitizer for SDT, since it would also be accumulated to normal cells in the vicinity of the tumors and would react to ultrasound stimulus. Thus, it is important to prepare TiO_2 NPs, which are selectively accumulated to only target cancer cells.

Two other groups have applied the sonocatalytic effect of TiO_2 NPs to *in vitro* cancer cell injury [28,29]. In their reports, TiO_2 NPs were not modified with biomolecules for targeting specific cells. With regard to their ultrasonic conditions, 1 MHz ultrasound was irradiated for 10–50 s at the intensity of 1.0 W/cm^2, which was several times higher than in the present study. The cell viability was reduced to 50% of the control just after the TiO_2/US treatment, and was about 10% of the control at 24 h after the treatment. Yamaguchi et al. [28] revealed that cell injury by their TiO_2/US treatment was mainly attributed to physical factors such as shear stress (not to chemical factors such as ROS), judging from the experiment using glutathione as the radical scavenger. Thus it was supposed that in their TiO_2/US treatment condition, the membrane integrity of most cells was immediately disrupted by physical factors such as shear stress (namely, necrotic cell death), although a part of the treated cells exhibited the early-stage apoptotic phenotype at 24 h after the treatment.

On the other hand, in the present study employing the 1 MHz ultrasound for 30 s at 0.1 W/cm^2, the cell viability remained at 80–100% of the control until 24 h after the TiO_2/US treatment, and then dropped afterward (Fig. 5). In this sense, it was considered that the TiO_2/US treatment examined in this study did not induce necrotic cell death, but apoptotic cell death (Fig. 6) due to the physical (shear stress) and chemical factor (OH radical) generated by the combination of lower intensity ultrasound and TiO_2 NPs localized to the cells.

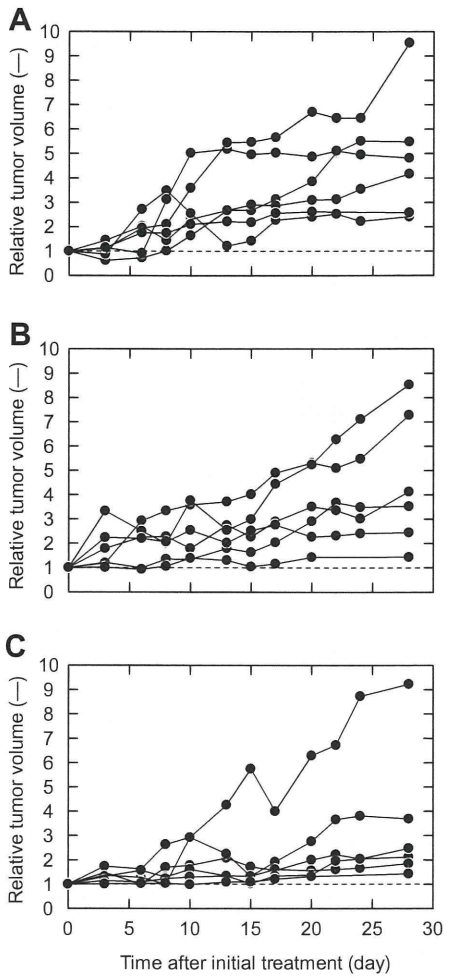

Fig. 7. Time courses of relative tumor volume on mouse xenograft model. TiO_2/US treatment was repeated five times at days 0, 3, 6, 10 and 13. (A) Control group without treatment; (B) group with ultrasound irradiation only; (C) group with TiO_2/US treatment. Each group had six mice. The dotted lines indicate unity of the relative tumor volume.

As for application of the sonocatalytic effect of TiO_2 NPs to *in vivo* cancer therapy, Harada et al. [29] first validated its practicability using a mouse xenograft model. In their study, 0.05 mg of TiO_2 NPs was injected directly into tumors, followed by 1 MHz ultrasound irradiation at 1.0 W/cm^2 for 120 s. Their TiO_2/US treatments were repeated five times during 8 days and resulted in the suppression of subsequent tumor growth compared with the control conditions, but could not achieve the regression of tumors within 21 days. In the present study, similar therapeutic results were obtained by the TiO_2/US treatment repeated five times during 13 days, by injecting 0.1 mg of pre-S1/S2-immobilized TiO_2 NPs and irradiating 1 MHz ultrasound at 1.0 W/cm^2 for 60 s (Fig. 7).

To enhance the anti-tumor effect of TiO_2/US treatment and realize complete regression, it might be necessary to accumulate much more TiO_2 NPs in the tumor regions. If TiO_2 NPs are injected via the tail vein, then many more targeting biomolecules should be immobilized on the NPs to improve the biodistribution of the NPs to tumors. With regard to ultrasound irradiation, it is better to employ the improved irradiation methodology for TiO_2/US treatment, such as the superimposition of dual ultrasounds [37,38], which can achieve a more efficient sonocatalytic reaction while maintaining the low-intensity of each ultrasound.

5. Conclusions

The availability of SDT using protein-immobilized TiO_2 NPs was examined *in vitro* and *in vivo*. The present study clarified the *in vitro* behavior of pre-S1/S2-mediated uptake of TiO_2 NPs by HepG2 cells. Moreover, this study also revealed the effect of TiO_2/US treatment on the immediate apoptosis induction and subsequent growth behavior of HepG2 cells. Finally, the TiO_2/US treatment could be applied to *in vivo* tumor therapy using a mouse xenograft model. For complete regression of tumors *in vivo*, further improvement of the TiO_2/US treatment is needed.

Acknowledgements

The present work was supported in part by a Grant-in-Aid for Scientific Research (B) (No. 19300182 to N.S.) from the Ministry of Education, Culture, Sports, Science and Technology, Japan.

References

[1] T.J. Mason, Therapeutic ultrasound an overview, Ultrason. Sonochem. 18 (2011) 847–852.
[2] J.E. Kennedy, High-intensity focused ultrasound in the treatment of solid tumours, Nat. Rev. Cancer 5 (2005) 321–327.
[3] T. Yu, Z. Wang, T.J. Mason, A review of research into the uses of low level ultrasound in cancer therapy, Ultrason. Sonochem. 11 (2004) 95–103.
[4] I. Rosenthal, J.Z. Sostaric, P. Riesz, Sonodynamic therapy–a review of the synergistic effects of drugs and ultrasound, Ultrason. Sonochem. 11 (2004) 349–363.
[5] M. Kuroki, K. Hachimine, H. Abe, H. Shibaguchi, S.I. Maekawa, J. Yanagisawa, T. Kinugasa, T. Tanaka, Y. Yamashita, Sonodynamic therapy of cancer using novel sonosensitizers, Anticancer Res. 27 (2007) 3673–3678.
[6] N. Yumita, R. Nishigaki, K. Umemura, Shin-ichiro umemura, hepatoporphyrin as a sensitizer of cell-damaging effect of ultrasound, Jpn. J. Cancer Res. 80 (1989) 219–222.
[7] T.J. Dougherty, J.E. Kaufman, A. Goldfarb, T.J. Dougherty, J.E. Kaufman, A. Goldfarb, K.R. Weishaupt, D. Boyle, A. Mittleman, Photoradiation therapy for the treatment of malignant tumors photoradiation therapy for the treatment of malignant tumors, Cancer Res. 38 (1978) 2628–2635.
[8] A. Fujishima, K. Honda, Electrochemical photolysis of water at a semiconductor electrode, Nature 238 (1972) 37–38.
[9] A. Fujishima, T.N. Rao, D.A. Tryk, Titanium dioxide photocatalysis, J. Photochem. Photobiol. C: Photochem. Rev. 1 (2000) 1–21.
[10] R. Cai, K. Hashimoto, I. Kiminori, Y. Kubota, A. Fujishima, Photokilling of malignant cells with ultrafine TiO_2 powder, Bull. Chem. Soc. Jpn. 64 (1991) 1268–1273.
[11] R. Cai, Y. Kubota, T. Shuin, R. Cai, Y. Kubota, T. Shuin, H. Sakai, K. Hashimoto, A. Fujishima, Induction of cytotoxicity by photoexcited TiO_2 particles advances in brief, Cancer Res. 52 (1992) 2346–2348.
[12] Y. Kubota, T. Shuin, C. Kawasaki, M. Hosaka, H. Kitamura, R. Cai, H. Sakai, K. Hashimoto, A. Fujishima, Photokilling of T-24 human bladder cancer cells with titanium dioxide, Br. J. Cancer 70 (1994) 1107–1111.
[13] A.-P. Zhang, Y.-P. Sun, Photocatalytic killing effect of TiO_2 nanoparticles on Ls-174-t human colon carcinoma cells, World J. Gastroenterol. 10 (2004) 3191–3193.
[14] J.-wook. Seo, H. Chung, M.-yun. Kim, J. Lee, I.-hong. Choi, J. Cheon, Development of water-soluble single-crystalline TiO2 nanoparticles for photocatalytic cancer-cell treatment, Small 3 (2007) 850–853.
[15] S. Yamaguchi, H. Kobayashi, T. Narita, K. Kanehira, S. Sonezaki, Y. Kubota, S. Terasaka, Y. Iwasaki, Novel photodynamic therapy using water-dispersed TiO_2-polyethylene glycol compound: evaluation of antitumor effect on glioma cells and spheroids *in vitro*, Photochem. Photobiol. 86 (2010) 964–971.
[16] C. Wang, S. Cao, X. Tie, B. Qiu, A. Wu, Z. Zheng, Induction of cytotoxicity by photoexcitation of TiO_2 can prolong survival in glioma-bearing mice, Mol. Biol. Rep. 38 (2011) 523–530.
[17] J. Xu, Y. Sun, J. Huang, C. Chen, G. Liu, Y. Jiang, Y. Zhao, Z. Jiang, Photokilling cancer cells using highly cell-specific antibody-TiO_2 bioconjugates and electroporation, Bioelectrochemistry 71 (2007) 217–222.
[18] E.A. Rozhkova, I. Ulasov, B. Lai, N.M. Dimitrijevic, M.S. Lesniak, T. Rajh, A high-performance nanobio photocatalyst for targeted brain cancer therapy, Nano Lett. 9 (2009) 3337–3342.
[19] K. Matsui, M. Karasaki, M. Segawa, S.Y. Hwang, T. Tanaka, C. Ogino, A. Kondo, Biofunctional TiO_2 nanoparticle-mediated photokilling of cancer cells using UV irradiation, Med. Chem. Commun. 1 (2010) 209–211.
[20] N. Shimizu, C. Ogino, M.F. Dadjour, K. Ninomiya, A. Fujihira, K. Sakiyama, Sonocatalytic facilitation of hydroxyl radical generation in the presence of TiO2, Ultrason. Sonochem. 15 (2008) 988–994.
[21] J. Wang, B. Guo, X. Zhang, Z. Zhang, J. Han, J. Wu, Sonocatalytic degradation of methyl orange in the presence of TiO_2 catalysts and catalytic activity comparison of rutile and anatase, Ultrason. Sonochem. 12 (2005) 331–337.

[22] N. Shimizu, C. Ogino, M.F. Dadjour, T. Murata, Sonocatalytic degradation of methylene blue with TiO_2 pellets in water, Ultrason. Sonochem. 14 (2007) 184–190.
[23] M. Stevenson, K. Bullock, W.-Y. Lin, K. Rajeshwar, Sonolytic enhancement of the bactericidal activity of irradiated titanium dioxide suspensions in water, Res. Chem. Intermed. 23 (1997) 311–322.
[24] M. Kubo, R. Onodera, N. Shibasaki-Kitakawa, K. Tsumoto, T. Yonemoto, Kinetics of ultrasonic disinfection of *Escherichia coli* in the presence of titanium dioxide particles, Biotechnol. Prog. 21 (2005) 897–901.
[25] M. Dadjour, C. Ogino, S. Matsumura, N. Shimizu, Kinetics of disinfection of by catalytic ultrasonic irradiation with TiO_2, Biochem. Eng. J. 25 (2005) 243–248.
[26] N. Shimizu, K. Ninomiya, C. Ogino, M.M. Rahman, Potential uses of titanium dioxide in conjunction with ultrasound for improved disinfection, Biochem. Eng. J. 48 (2010) 416–423.
[27] C. Ogino, N. Shibata, R. Sasai, K. Takaki, Y. Miyachi, Shun-ichi Kuroda, K. Ninomiya, N. Shimizu, Construction of protein-modified TiO_2 nanoparticles for use with ultrasound irradiation in a novel cell injuring method, Bioorg. Med. Chem. Lett. 20 (2010) 5320–5325.
[28] S. Yamaguchi, H. Kobayashi, T. Narita, K. Kanehira, S. Sonezaki, N. Kudo, Y. Kubota, S. Terasaka, K. Houkin, Sonodynamic therapy using water-dispersed TiO_2-polyethylene glycol compound on glioma cells: comparison of cytotoxic mechanism with photodynamic therapy, Ultrason. Sonochem. 18 (2011) 1197–1204.
[29] Y. Harada, K. Ogawa, Y. Irie, H. Endo, L.B. Feril, T. Uemura, K. Tachibana, Ultrasound activation of TiO_2 in melanoma tumors, J. Control. Release 149 (2011) 190–195.
[30] T. Yamada, Y. Iwasaki, H. Tada, H. Iwabuki, M.K.L. Chuah, T. VandenDriessche, H. Fukuda, A. Kondo, M. Ueda, M. Seno, K. Tanizawa, S. Kuroda, Nanoparticles for the delivery of genes and drugs to human hepatocytes, Nat. Biotechnol. 21 (2003) 885–890.
[31] T. Kasuya, T. Yamada, A. Uyeda, T. Matsuzaki, T. Okajima, K. Tatematsu, K. Tanizawa, S. Kuroda, In vivo protein delivery to human liver-derived cells using hepatitis B virus envelope pre-S region, J. Biosci. Bioeng. 106 (2008) 99–102.
[32] K. Kanehira, T. Banzai, C. Ogino, N. Shimizu, Y. Kubota, S. Sonezaki, Properties of TiO_2-polyacrylic acid dispersions with potential for molecular recognition, Colloids Surf. B. Biointerfaces 64 (2008) 10–15.
[33] D.R. Schultz, W.J. Harrington, Apoptosis: programmed cell death at a molecular level, Semin. Arth. Rheum. 32 (2003) 345–369.
[34] D.M. Euhus, C. Hudd, M.C. LaRegina, F.E. Johnson, Tumor measurement in the nude mouse, J. Surg. Oncol. 31 (1986) 229–234.
[35] L. Lagneaux, E.C. de Meulenaer, A. Delforge, M. Dejeneffe, M. Massy, C. Moerman, B. Hannecart, Y. Canivet, M.F. Lepeltier, D. Bron, Ultrasonic low-energy treatment: a novel approach to induce apoptosis in human leukemic cells, Exp. Hematol. 30 (2002) 1293–1301.
[36] L.B. Feril, T. Kondo, Z.-G. Cui, Y. Tabuchi, Q.-L. Zhao, H. Ando, T. Misaki, H. Yoshikawa, S. Umemura, Apoptosis induced by the sonomechanical effects of low intensity pulsed ultrasound in a human leukemia cell line, Cancer Lett. 221 (2005) 145–152.
[37] K. Kawabata, Effect of second-harmonic superimposition on efficient induction of sonochemical effect, Ultrason. Sonochem. 3 (1996) 1–5.
[38] S. Umemura, K. Kawabata, K. Sasaki, *In vitro* and *in vivo* enhancement of sonodynamically active cavitation by second-harmonic superimposition, J. Acoust. Soc. Am. 101 (1997) 569–577.

analytical chemistry

LETTER

pubs.acs.org/ac

Coupling Stimuli-Responsive Magnetic Nanoparticles with Antibody–Antigen Detection in Immunoassays

Hirokazu Nagaoka,[†] Yasunobu Sato,[†] Xiaomao Xie,[†] Hideyuki Hata,[†] Masaru Eguchi,[†] Nobuki Sakurai,[†] Takeshi Watanabe,[†] Hiroshi Saitoh,[†] Akihiko Kondo,[§] Satoru Sugita,[*,‡] and Noriyuki Ohnishi[*,†]

[†]JNC Petrochemical Corporation, Goi Research Center, 5-1 Goi-kaigan, Ichihara, Chiba 290-8551, Japan

[‡]Ortho Clinical Diagnostics, 3-5-2 Nishi-kanda, Chiyoda-ku, Tokyo 101-0065, Japan

[§]Department of Chemical Science and Engineering, Graduate School of Engineering, Kobe University, 1-1 Rokkodaicho, Nada-ku, Kobe, Hyogo 657-8501, Japan

Supporting Information

ABSTRACT: Because current homogeneous immunoassays show some limitations, particularly low sensitivity, we developed a new immunoassay to overcome these limitations. The approach was based on magnetic nanoparticles with a thermoresponsive polymer layer, a negatively charged polymer, and streptavidin–biotin-based antibody–antigen detection and yielded higher sensitivity than commonly used heterogeneous immunoassays. Because no special equipment is needed, it can be applied to currently available absorbance-based systems for high-throughput assays.

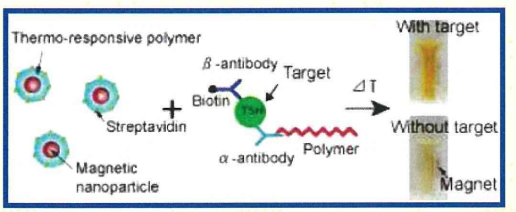

Homogeneous immunoassays such as latex agglutination assays require only mixing of a sample and immunochemical reagents followed by detection. The antigen–antibody binding produces a physically detectable signal, overcoming the need to separate bound from free labeled analytes. This approach minimizes the requirements for automation, an advantage in high-throughput immunoassays.[1,2] However, many disease markers are found at low levels in body fluids necessitating highly sensitive heterogeneous approaches, such as chemiluminescence enzyme immunoassays (CLEIA) and electrochemiluminescent immunoassay (ECLIA) using magnetic particles.[3−5] Although homogeneous immunoassays are becoming more widely used, they show poor sensitivity for samples with low marker concentrations where the particle concentration exceeds that of the marker. In this situation, it is necessary to quantify the formation of pairs of particles (doublets).[6] However, there are two limitations when doublets are used as the signal for detection.

The first limitation is the resolution of doublets. For latex agglutination assays, turbidimetry is often used to discriminate doublets, which scatter twice as much light as two single particles would. However, the scattering from single particles will add to the signal from the doublets because homogeneous immunoassays have no separation step. Therefore, the number of doublets that can be detected is ultimately limited by the total number of particles in the solution. The second limitation is the collision frequency of particles. Because of the resolution limitation, there is a need to decrease the particle concentration to increase sensitivity. However, decreasing the number of particles involved in the reaction solution increases the time needed for an effective reaction to take place. In fact, when the antibody–antigen reaction is used for cross-linking particles, as in latex agglutination assays, the number of effective collisions that develop doublets is reaction-limited.[7]

Several approaches have been proposed to improve the sensitivity of homogeneous immunoassays. The limited resolution of the doublets can be improved by precisely counting nonaggregated particles, as in particle agglutination counting immunoassays.[8] Individual particles in a flowing stream are detected with a laser beam, and the number of nonaggregated particles is counted based on their distinct scattering patterns. Another way to improve resolution is based on the luminescent oxygen channeling immunoassay (LOCI) technique, which detects the formation of particle pairs rather than large aggregates and measures photochemically triggered chemiluminescence.[9] The limited collision frequency associated with latex agglutination assays has been overcome by applying an external force, such as ultrasonic waves,[10] magnetic fields,[11] and electric fields,[12] to the particles to increase collision frequency. Using these approaches, proteins can be detected at picomolar concentrations. Although these approaches have improved the detection limits of homogeneous immunoassays, no single method has overcome both limitations.

Therefore, we developed a strategy to detect markers without relying on the formation of doublets, relying instead on the inhibition of particle aggregation through antigen–antibody recognition. We used stimuli-responsive magnetic nanoparticles (MNPs) (Therma-Max), which consist of a stimuli-responsive polymer coating on the surface of the particle. Stimuli-responsive polymers are polymers that respond to small changes in their

Received: July 14, 2011
Accepted: November 9, 2011
Published: November 09, 2011

dx.doi.org/10.1021/ac201814n | *Anal. Chem.* 2011, 83, 9197–9200

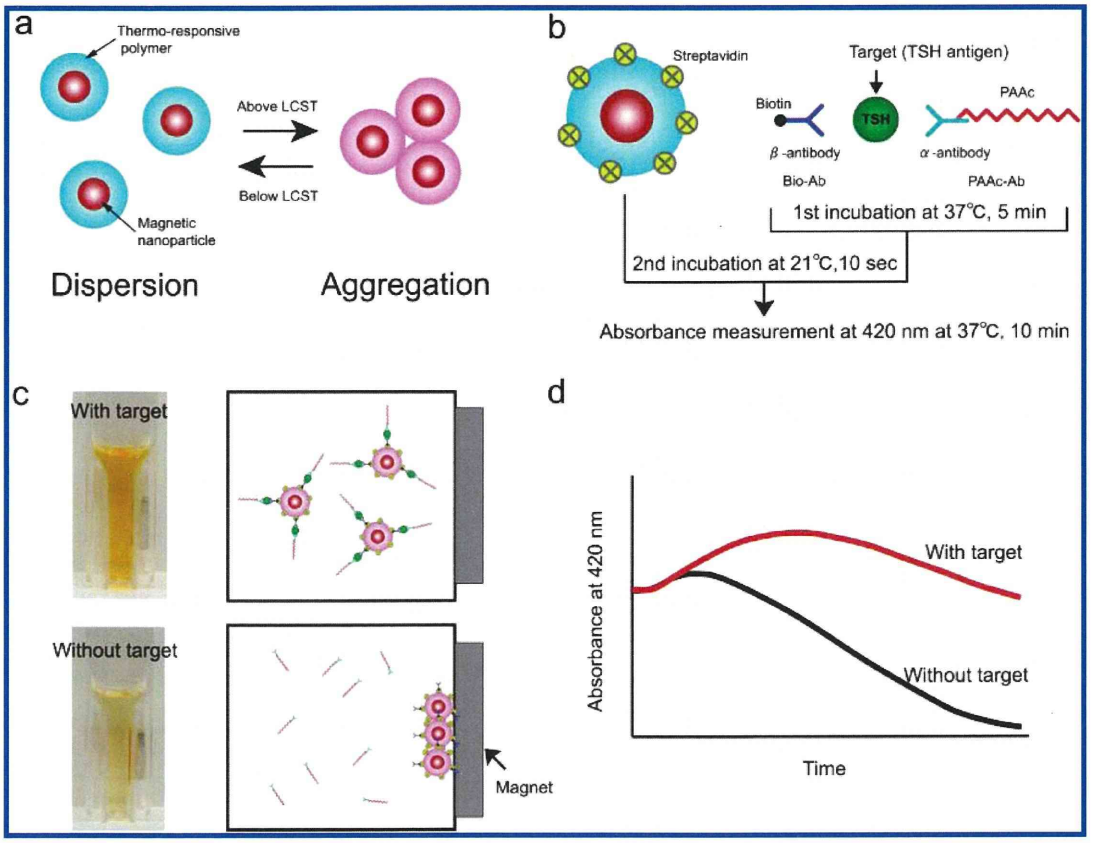

Figure 1. Schematic representation of the polarity variation immunoassay (PVIA). (a) Characteristics of the thermoresponsive magnetic nanoparticles (MNPs). (b) The protein marker (TSH) is sandwiched between biotinylated primary β-antibody (Bio-Ab) and PAAc-conjugated secondary α-antibody (PAAc-Ab) and forms a Bio-Ab−antigen−PAAc-Ab complex during the first incubation. Then, it is reacted with thermoresponsive magnetic nanoparticles coated with streptavidin. (c) Photograph of the cuvette, with a magnet attached, after the PVIA experiment and illustration of the reaction taking place inside the cuvette maintained at a temperature of 37 °C. In the presence of the marker, the complex is bound to the surface of the MNPs and aggregation of the MNPs is inhibited. In the absence of the marker, the MNP aggregates are quickly removed with the magnet. (d) Typical results showing the change in absorbance at 420 nm.

environment such as temperature and pH.[13] These polymers, such as poly(*N*-isopropylacrylamide) (PNIPAAm), are soluble in an aqueous solution below their lower critical solution temperature (LCST) and precipitate above their LCST. MNPs have an average diameter of 100 nm and show reversible transition between aggregation and dispersion across the LCST (Figure 1a). Nanosized magnetic particles respond weakly to a magnet because of their random Brownian motion. When the temperature increases above their LCST, the MNPs begin to aggregate, which increases their size and the aggregated particles can be removed quickly from the solution with a magnet.[14,15] Because of the presence of a thermoresponsive polymer, small changes around the surface of the particle affect the type of response. We developed a system in which the constituents are streptavidin-labeled MNPs, poly(acrylic acid) (PAAc) conjugated to an antibody (PAAc-Ab), and a biotin-labeled β antibody (biotin-Ab) (Figure 1b). As summarized in Figure 1c, in the absence of a protein marker, streptavidin-labeled MNPs aggregate and are removed from solution by a magnet. In the presence of the protein marker, the marker is sandwiched between PAAc-Ab and biotin-Ab and the sandwiched complexes are bound to individual MNPs through streptavidin−biotin binding. This prevents aggregation based on changes in the polarity in the vicinity of the thermoresponsive polymer, and the MNPs are not removed from solution by a magnet. We called this method the polarity variation immunoassay (PVIA).

This approach was designed to solve two problems. First, the inhibition of aggregation of MNPs is detected with high sensitivity by observing the removal velocity of the aggregated MNPs. Therefore, the detection limit is improved from the point of resolution. Second, PVIA provides shorter assay runtime because the aggregation of MNPs is rapid above the LCST.

To demonstrate our method, we used thyroid stimulating hormone (TSH) as a model to test the detection limit and dynamic range of PVIA. As shown in Figure 1b, we first mixed the sample with the Bio-Ab and PAAc-Ab at 37 °C. Next, streptavidin-labeled MNPs were added to this mixture and incubated at 21 °C. The resulting solution was transferred to a cuvette with a magnet attached to its side and placed in a spectrophotometer at 37 °C (experimental details are available in the Supporting Methods in the Supporting Information). Figure 1c,d shows the relationship between the reaction inside the cuvette and absorbance measured at 420 nm. There are two distinct phases: an initial small increase followed by a rapid decrease over time. The initial increase in absorbance is due to the phase-transition of the thermoresponsive polymer

dx.doi.org/10.1021/ac201814n |*Anal. Chem.* 2011, 83, 9197–9200

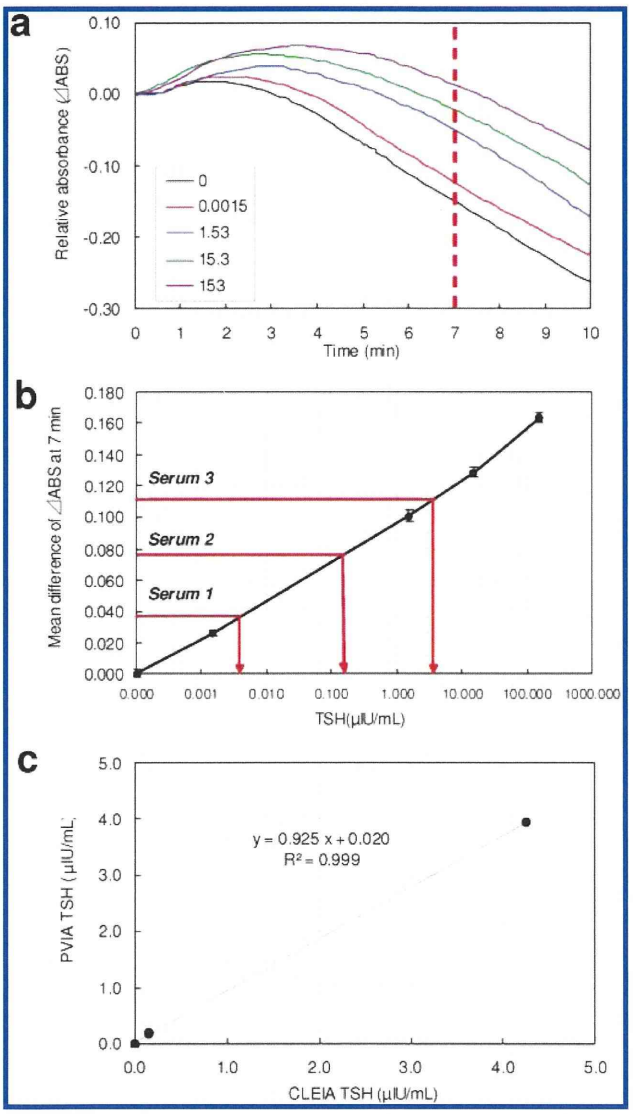

Figure 2. (a) Raw data showing the time-course of absorbance at 420 nm obtained with TSH calibrators at concentrations of 0, 0.0015, 1.53, 15.3, and 153 μIU/mL. (b) Calibration curve showing the mean difference in absorbance to 0 μIU/mL TSH at 7 min. The concentration of TSH in three patient samples was calculated using the calibration curve. (c) Correlation between PVIA and CLEIA for TSH concentrations in the three patient samples. Experimental protocols for PVIA and CLEIA are described in the Supporting Methods section.

coating the MNPs and the aggregation of the MNPs. The subsequent decrease in absorbance is due to removal of the aggregated MNPs from solution by the magnet. This phenomenon could be interpreted as follows: the MNPs have a LCST of around 22 °C and do not aggregate during the second incubation. However, transferring the solution to the spectrophotometer at 37 °C increased the temperature of the solution, and the MNPs aggregate and are removed from solution by the magnet. In the presence of TSH, PAAc-Ab binds to the surface of the MNPs, which inhibits aggregation through changes in the polarity in the vicinity of the thermoresponsive polymer, and this trend becomes more noticeable as the TSH concentration increases (Figure 2a).

Figure 2b shows the calibration curve of the PVIA with a TSH calibrator. The intra-assay CVs of the assay are below 4% (n = 3) (Supporting Table 1 in the Supporting Information). The limit of detection of this system was determined by a two-tailed Student t test between the signals at 0 and at 0.0015 μIU/mL. The two signal values are statistically different (p < 0.001). Therefore the limit of detection should be better than 0.0015 μIU/mL, which is 2 times more sensitive than heterogeneous CLEIA (0.0032 μIU/mL)[16] and 5 times more sensitive than homogeneous LOCI (0.007 μIU/mL; detection limit stated in the instruction manual of the Dimension TSHL Flex reagent cartridge). PVIA also has a wide detection range that avoids the need to dilute samples. To determine whether our PVIA is as reliable as other assays, we compared the PVIA results for TSH in three clinical samples with those obtained using CLEIA (VITROS [Ortho Clinical Diagnostics]; experimental details are available in the Supporting Methods in the Supporting Information). The results of both assays were similar (Figure 2c), demonstrating that our PVIA is adequate for measuring clinical samples. The total assay time was 12 min, as compared with 40 min for CLEIA (VITROS, TSH).

The main reason for the PVIA's high sensitivity is not yet fully understood, although two explanations seem feasible. First, the removal of aggregated MNPs improves discrimination between the aggregated and nonaggregated particles. In PVIA, the difference in flow velocity of the aggregated MNPs is measured using a magnet. The magnetically induced flow velocity, $\mathbf{u}_{mag}$, for MNPs is given by[17]

$$\mathbf{u}_{mag} \propto r^2 \chi_p \qquad (1)$$

where r is the particle radius and χ_p is the magnetic susceptibility of the particle. Flow velocity is sensitive to increases in particle size, being proportional to the square of the particle radius. Therefore, measurement of flow velocity is more sensitive than measuring particle size. The second reason is related to the aggregation of MNPs. MNPs below the LCST have a hydrophilic surface and the particles are sterically stabilized. However, as the temperature of the solution increases and crosses the LCST, the MNPs rapidly aggregate because the surface of the particles becomes hydrophobic above the LCST.

This process is diffusion-limited and is quicker than the reaction-limited aggregation in latex agglutination assays at low marker concentrations. Therefore, the aggregation of MNPs in PVIA is fast and will shorten the total assay time.

In summary, PVIA can overcome the limitations of conventional immunoassays. The molecular scale recognition step resulting from the formation of a small amount of antigen–antibody binding is transformed into a macroscopic signal through a cascade of physical events. We suggest that PVIA can be integrated with other assays in high-throughput automated systems.

■ ASSOCIATED CONTENT

Supporting Information. Experimental procedures of PVIA and the preparation of conjugates are included in supporting methods and additional information as noted in the text. This material is available free of charge via the Internet at http://pubs.acs.org.

dx.doi.org/10.1021/ac201814n |Anal. Chem. 2011, 83, 9197–9200

AUTHOR INFORMATION

Corresponding Author

*Noriyuki Ohnishi: phone, +81-436-21-5127; fax, +81-436-23-0381; e-mail, onishi@jnc-corp.co.jp. Satoru Sugita: phone, +81-3-4411-7029; fax, +81-3-4411-7711; e-mail, ssugita@its.jnj.com.

REFERENCES

(1) Wild, D. *The Immunoassay Handbook*, 3rd ed.; Elsevier Ltd.: Oxford, U.K., 2005.

(2) Gosling, J. P. *Clin. Chem.* **1990**, *36*, 1408–1427.

(3) Sokoll, L. J.; Chan, D. W. *Anal. Chem.* **1999**, *71*, 356R–362R.

(4) Tang, D.; Yuan, R.; Chai, Y. *Biotechnol. Lett.* **2006**, *28*, 559–565.

(5) Tsai, H. Y.; Hsu, C. F.; Chiu, I.; Bor Fuh, W. C. *Anal. Chem.* **2007**, *79*, 8416–8419.

(6) Baudry, J.; Rouzeau, C.; Goubault, C.; Robic, C.; Cohen-Tannoudji, L.; Koenig, A.; Bertrand, E.; Bibette, J. *Proc. Natl. Acad. Sci. U.S.A.* **2006**, *103*, 16076–16078.

(7) Stoll, S.; Lanet, V.; Pefferkorn, E. *J. Colloid Interface Sci.* **1993**, *157* 302–311.

(8) Masson, P. L.; Cambiaso, C. L.; Collet-Cassart, D.; Magnusson, C. G.; Richards, C. B.; Sindic, C. J. *Methods Enzymol.* **1981**, *74*, 106–139.

(9) Ullman, E. F.; Kirakossian, H.; Switchenko, A. C.; Ishkanian, J.; Ericson, M.; Wartchow, C. A.; Pirio, M.; Pease, J.; Irvin, B. R.; Singh, S; Singh, R.; Patel, R.; Dafforn, A.; Davalian, D.; Skold, C.; Kurn, N.; Wagner, D. B. *Clin. Chem.* **1996**, *42*, 1518–1526.

(10) Ellis, R. W.; Sobanski, M. A. *J. Med. Microbiol.* **2000**, *49* 853–859.

(11) Song, M. I.; Iwata, K.; Yamada, M.; Yokoyama, K.; Takeuchi, T.; Tamiya, E.; Karube, I. *Anal. Chem.* **1994**, *66*, 778–781.

(12) Negi, A. S.; Sood, A. K. *Clin. Chem.* **2008**, *54*, 366–370.

(13) Hoffman, A. S.; Stayton, P. S.; Bulmus, V.; Chen, G.; Chen, J.; Cheung, C.; Chilkoti, A.; Ding, Z.; Dong, L.; Fong, R.; Lackey, C. A.; Long, C. J.; Miura, M.; Morris, J. E.; Murthy, N.; Nabeshima, Y.; Park, T. G.; Press, O. W.; Shimoboji, T.; Shoemaker, S.; Yang, H. J.; Monji, N.; Nowinski, R. C.; Cole, C. A.; Priest, J. H.; Harris, J. M.; Nakamae, K.; Nishino, T.; Miyata, T. *J. Biomed. Mater. Res.* **2000**, *52*, 577–586.

(14) Kondo, A.; Kamura, H.; Higashitani, K. *Appl. Microbiol. Biotechnol.* **1994**, *41*, 99–105.

(15) Ohnishi, N.; Furukawa, H.; Hideyuki, H.; Wang, J.; An, C.; Fukusaki, E.; Kataoka, K.; Ueno, K.; Kondo, A. *Nanobiotechnology* **2006**, *2*, 43–49.

(16) Saw, S.; Sethi, S.; Aw, T. C. *Clin. Chem.* **1999**, *45*, 578–580.

(17) Pamme, N.; Manz, A. *Anal. Chem.* **2004**, *76*, 7250–7256.

the FEBS Journal

Gγ recruitment system incorporating a novel signal amplification circuit to screen transient protein-protein interactions

Nobuo Fukuda[1], Jun Ishii[2] and Akihiko Kondo[1]

1 Department of Chemical Science and Engineering, Graduate School of Engineering, Kobe University, Japan
2 Organization of Advanced Science and Technology, Kobe University, Japan

Keywords
Gγ recruitment system; G-protein signal; mating; transient protein–protein interactions; yeast

Correspondence
A. Kondo, Department of Chemical Science and Engineering, Graduate School of Engineering, Kobe University, 1-1 Rokkodaicho, Nada-ku, Kobe 657-8501, Japan
Fax: +81 78 803 6196
Tel: +81 78 803 6196
E-mail: akondo@kobe-u.ac.jp

(Received 5 April 2011, revised 20 May 2011, accepted 5 July 2011)

doi:10.1111/j.1742-4658.2011.08232.x

Weak and transient protein–protein interactions are associated with biological processes, but many are still undefined because of the difficulties in their identification. Here, we describe a redesigned method to screen transient protein–protein interactions by using a novel signal amplification circuit, which is incorporated into yeast to artificially magnify the signal responding to the interactions. This refined method is based on the previously established Gγ recruitment system, which utilizes yeast G-protein signaling and mating growth selection to screen interacting protein pairs. In the current study, to test the capability of our method, we chose mutants of the Z-domain derived from *Staphylococcus aureus* protein A as candidate proteins, and the Fc region of human IgG as the counterpart. By introduction of an artificial signal amplifier into the previous Gγ recruitment system, the signal transduction responding to transient interactions between Z-domain mutants and the Fc region with significantly low affinity (8.0×10^3 M^{-1}) was successfully amplified in recombinant haploid yeast cells. As a result of zygosis with the opposite mating type of wild-type haploid cells, diploid colonies were vigorously and selectively generated on the screening plates, whereas our previous system rarely produced positive colonies. This new approach will be useful for exploring the numerous transient interactions that remain undefined because of the lack of powerful screening tools for their identification.

Introduction

Protein–protein interactions are essential for most biological processes in the cell. Although various approaches, including yeast two-hybrid systems, have succeeded in the identification of numerous interactions, many interactions still remain undefined. Representative of such cases are interactions with low affinities, as it is difficult to capture transient interactions switching between associated and dissociated states. However, weak and transient interactions should be investigated more intensely, because they are likely to be functionally important in biological processes, and can potentially provide important new insights into molecular mechanisms [1].

Yeast two-hybrid systems [2–6] are simple genetic *in vivo* technologies for screening and identification of protein interactions. In these techniques, protein–protein

Abbreviations
EGFR, epidermal growth factor receptor; EGFP, enhanced green fluorescent protein; GFP, green fluorescent protein; $G\gamma_{cyto}$, Gγ subunit with deletion of lipidation site; Z_{EGFR}, variant of the Z-domain with its binding target genetically altered from the Fc region to epidermal growth factor receptor; Z_{I31A}, single-site mutant of the Z-domain with Ile31 replaced by alanine; Z_{K35A}, single-site mutant of the Z-domain with Lys35 replaced by alanine; Z_{WT}, wild-type Z-domain derived from the B domain of *Staphylococcus aureus* protein A; ZZ, dimer of wild-type Z-domain.

interactions are conventionally detected on the basis of transcriptional activation that is restored via reconstitution of the split proteins divided into two regions. Commonly, screening of interacting positive clones from large-scale libraries can be performed by using auxotrophic or drug-resistant reporter genes, such as *HIS3* [7] or *AUR1-C* [8], whereas their intensities might be evaluated by relative quantification of transcriptional levels with colorimetric, luminescent or fluorescent reporters, such as *lacZ* [2], *luc* [9], or green fluorescent protein (*GFP*) [10]. Although there is no doubt that yeast two-hybrid systems are powerful tools for elucidating interacting protein targets, it is still a challenge to establish methods for screening weak and transient interactions. Therefore, a powerful approach to screen transient interactions is required for understanding of their biological roles.

We previously developed the 'Gγ recruitment system', which utilizes yeast G-protein signaling (pheromone signaling) to detect protein–protein interactions [11–13]. This system can avoid the appearance of background response for noninteracting protein pairs, because it is based on the biological phenomenon that signal transduction requires localization of the Gβγ complex to the inner leaflet of the plasma membrane through a lipidated Gγ subunit in yeast [14]. Whereas deletion of lipidation sites in yeast Gγ ($G\gamma_{cyto}$) completely interrupts G-protein signaling [13], protein–protein interactions between the $G\gamma_{cyto}$-fused target (Y) and membrane-bound candidate (X) lead to the recruitment of $G\gamma_{cyto}$ towards the plasma membrane and results in the functional recovery of G-protein signaling (Fig. 1A) [11–13]. As the outputs appear as various mating responses, including global changes in transcription, a reporter gene assay and mating selection are available (Fig. 1A) [12].

Unlike stable interactions, however, transient interactions cannot generally transmit enough signals to generate clear outputs, and it would therefore be difficult to screen transient interactions. In the current study, we therefore redesigned the previous Gγ recruitment system to amplify negligible signals in response to transient protein–protein interactions by incorporating a novel signal amplification circuit. As

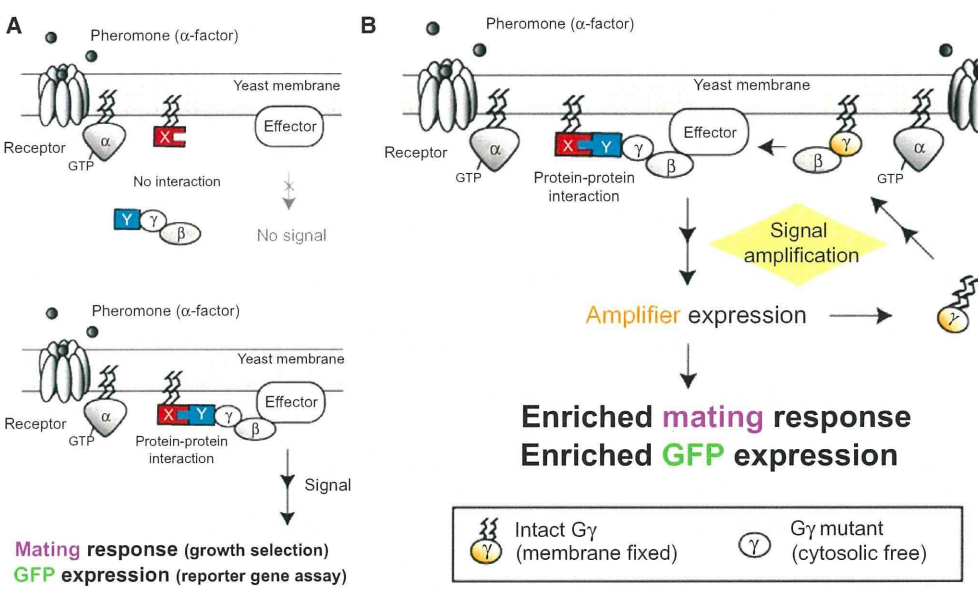

Fig. 1. Schematic outline of experimental design. (A) Previously established Gγ recruitment system to detect protein–protein interactions. Engineered Gγ lacking membrane localization ability ($G\gamma_{cyto}$) is genetically prepared and substituted for the endogenous Gγ, resulting in interruption of signal transduction owing to cytosolic translocation of the Gβ subunit from the membrane. The binding candidate 'X' is located on the inner leaflet of the plasma membrane, and the binding target 'Y' is fused to cytosolic $G\gamma_{cyto}$. The X–Y interaction restores the G-protein signal by recruiting $G\gamma_{cyto}$ accompanied by Gβ towards the plasma membrane, and it therefore allows for cellular changes in the mating process. Therefore, the generation of diploid cells with opposite mating-type cells can be used to screen interacting protein pairs, or pheromone-responsive transcription of a *GFP* reporter gene can be used to estimate the signaling levels corresponding to X–Y interactions. (B) New approach incorporating a signal amplification circuit into the Gγ recruitment system to screen transient protein–protein interactions. The G-protein signal induced by the X–Y interaction is amplified by signal-responsive expression of intact Gγ (artificial signal amplifier). As a consequence, the enriched mating response permits practicable selection of the transient X–Y interaction, or GFP expression can be used to estimate the signaling levels.

the artificial signal amplifier, we utilized intact Gγ, which can localize at the plasma membrane by itself. If the intact Gγ is designed to be expressed in response to the signaling transmission, the expressed Gγ will participate in activation of the signaling and continuously amplify the signal transduction (Fig. 1B). Therefore, the mating responses should be highly enriched, even in cases of transient interactions (Fig. 1B). We herein show the feasibility of this approach and its powerful ability to screen weak and transient protein–protein interactions.

Results and Discussion

Design of a novel signal amplification circuit to screen transient interacting protein pairs

The aim of this study was to establish and validate a screening method for weak and transient protein–protein interactions by utilizing the Gγ recruitment system as a basic scaffold (Fig. 1A) [11]. In our previous study, a growth selection technique based on diploid formation in the yeast mating machinery to screen interacting protein pairs without expensive instruments was successfully established [12]. However, as the binding strength significantly affects the recruitment of the Gβγ complex to the plasma membrane (Fig. 1A) [12], transient interactions might not transmit enough signals to form diploid cells.

To address this problem, the previous Gγ recruitment system was redesigned to amplify the signals responding to protein–protein interactions by incorporation of a novel signal amplification circuit (Fig. 1B). With intact Gγ as the amplifier, we refined the Gγ recruitment system to express the *STE18* gene (encoding intact Gγ) in a pheromone-responsive manner (Table 1). In response to X–Y interactions, the expressed Gγ will localize at the plasma membrane and form a complex with free Gβ, which directly activates subsequent signaling on the inner leaflet of the yeast plasma membrane (Fig. 1B). Therefore, the amount of Gβγ complex, which can localize at the membrane and participate in signal transduction, should increase in this circuit (Fig. 1B). As a consequence, a negligible signal will be continuously amplified and the enriched mating responses will allow for screening of transient protein–protein interactions.

As interacting protein pairs, the Fc region of human IgG and the Z-domain derived from *Staphylococcus aureus* protein A were selected [15,16], as the Z-domain has a number of variants with a wide range of affinity constants for the Fc region, such as the single-site mutant of the Z-domain with Ile31 replaced by alanine (Z_{I31A}) (8.0×10^3 M^{-1}), the single-site mutant of the Z-domain with Lys35 replaced by alanine (Z_{K35A}) (4.6×10^6 M^{-1}), the wild-type Z-domain (Z_{WT}) (5.9×10^7 M^{-1}), and the dimer of Z_{WT} (ZZ) (6.8×10^8 M^{-1}) [17]. With Z_{I31A} and Fc as a model for the transient interactions, we tested the applicability of our method with mating growth selection on diploid selection plates.

Diploid growth selection to screen transient interacting protein pairs with an artificial signal amplifier

Yeast haploid strains BY4741 (**a** mating-type) and BY4742 (α mating-type), which, respectively, require

Table 1. List of the yeast strains used in this study.

Strain	Genotype	Reference
BY4741	*MATa his3Δ1 ura3Δ0 leu2Δ0 met15Δ0*	Brachmann *et al.* [18]
BFG2118	BY4741 P_{FIG1}-*FIG1-EGFP ste18Δ::kanMX4 his3Δ::URA3-*P_{STE18}-$G\gamma'_{cyto}$-*Fc*	Fukuda *et al.* [11]
BFG2Z18-I31A	BY4741 P_{FIG1}-*FIG1-EGFP ste18Δ::kanMX4-*P_{PGK1}-$Z_{I31A,mem}$ *his3Δ::URA3-*P_{STE18}-$G\gamma'_{cyto}$-*Fc*	Fukuda *et al.* [11]
BFG2Z18-K35A	BY4741 P_{FIG1}-*FIG1-EGFP ste18Δ::kanMX4-*P_{PGK1}-$Z_{K35A,mem}$ *his3Δ::URA3-*P_{STE18}-$G\gamma'_{cyto}$-*Fc*	Fukuda *et al.* [11]
BFG2Z18-WT	BY4741 P_{FIG1}-*FIG1-EGFP ste18Δ::kanMX4-*P_{PGK1}-$Z_{WT,mem}$ *his3Δ::URA3-*P_{STE18}-$G\gamma'_{cyto}$-*Fc*	Fukuda *et al.* [11]
BZFG2118	BY4741 P_{FIG1}-*FIG1-EGFP ste18Δ::kanMX4-*P_{PGK1}-ZZ_{mem} *his3Δ::URA3-*P_{STE18}-$G\gamma'_{cyto}$-*Fc*	Fukuda *et al.* [11]
FG0	BFG2118 P_{HOP2}*::LEU2-*P_{FIG1}-$G\gamma$	Present study
FG1	BFG2Z18-I31A P_{HOP2}*::LEU2-*P_{FIG1}-$G\gamma$	Present study
FG2	BFG2Z18-K35A P_{HOP2}*::LEU2-*P_{FIG1}-$G\gamma$	Present study
FG3	BFG2Z18-WT P_{HOP2}*::LEU2-*P_{FIG1}-$G\gamma$	Present study
FG4	BZFG2118 P_{HOP2}*::LEU2-*P_{FIG1}-$G\gamma$	Present study
FG-955	BY4741 P_{FIG1}-*FIG1-EGFP ste18Δ::kanMX4-*P_{PGK1}-$Z_{EGFR,mem}$ *his3Δ::URA3-*P_{STE18}-$G\gamma'_{cyto}$-*Fc* P_{HOP2}*::LEU2-*P_{FIG1}-$G\gamma$	Present study
FG-HXT	BY4741 P_{FIG1}-*FIG1-EGFP ste18Δ::kanMX4-*P_{PGK1}-*HXT1 his3Δ::URA3-*P_{STE18}-$G\gamma'_{cyto}$-*Fc* P_{HOP2}*::LEU2-*P_{FIG1}-$G\gamma$	Present study
BY4742	*MATα his3Δ1 ura3Δ0 leu2Δ0 lys2Δ0*	Brachmann *et al.* [18]

methionine or lysine for growth, [18], were utilized as parental strains for mating. Genetic modifications to evaluate the interactions of protein pairs were used only for BY4741 (Table 1). When protein–protein interactions occur in engineered **a** cells, they mate with intact **α** cells. The formation of diploid cells in medium lacking methionine and lysine depends on the affinities of the protein pairs [12].

To verify our hypothesis that the incorporation of a signal amplification circuit allows the selection of transient interactions, the full-length *STE18* gene (encoding intact Gγ) was introduced into five **a**-type *ste18*Δ strains (BFG2118, BFG2Z18-I31A, BFG2Z18-K35A, BFG2Z 18-WT, and BZFG2118) (Table 1), to be expressed under the control of the pheromone-responsive *FIG1* promoter [19,20]. In addition, the yielding strains, FG0, FG1, FG2, FG3, and FG4, constitutively expressed the $G\gamma_{cyto}$–Fc fusion protein and several membrane-localized Z-domain variants as interaction models with a wide range of affinity constants with the same genotypes as the parental strains (Table 1). Using the newly constructed strains and the previous strains, we investigated the correspondence of diploid formation and the protein interactions within several ranges of affinities (Fig. 2).

In the previous system, a negative control expressing only the $G\gamma_{cyto}$–Fc fusion protein in the *ste18*Δ strain (None–Fc) never exhibited diploid formation. In contrast, yeast strains that express the $G\gamma_{cyto}$–Fc fusion protein and several Z-domain variants (Z_{K35A}, Z_{WT}, and ZZ) mated with BY4742 and formed diploid cells. The capability for diploid formation was dependent on the affinities between Fc and Z-domain variants. In the case of the transient Z_{I31A}–Fc interaction (8.0×10^3 M^{-1}), the previous system rarely generated diploid cells, as expected. These data indicate that transient interactions cannot be isolated in a library-based screen with the Gγ recruitment system. Thus, an advanced approach is required to screen transient interactions *in vivo*.

As compared with the previous system, the current system, in which a signal amplification circuit was incorporated by using an artificial signal amplifier, generated increased numbers of diploid cells for all interactions (Fig. 2). Furthermore, we confirmed that the current system amplified the signaling levels responding to the Z_{I31A}–Fc interaction by measuring the transcriptions involved in the mating (Fig. 3). These results demonstrated that the novel signal amplification circuit successfully functioned to enhance the detection sensitivity of protein–protein interactions in our previous system. Especially for the transient Z_{I31A}–Fc interaction (8.0×10^3 M^{-1}), for which the previous system generated few or no diploid cells, the current system dramatically improved diploid cell formation (20 000-fold). As a consequence, our approach successfully permitted the growth isolation of the transient Z_{I31A}–Fc interaction on the selection medium, suggesting that library screening of transient interactions is as feasible as detecting strong and stable interactions in our current system.

Specificity for detection of protein–protein interactions

In general, highly sensitive systems might detect even undesirable, feeble signals. To confirm the specificity of detection of protein–protein interactions in our method, we investigated the activation levels of G-protein signaling by altering the counterparts of the Fc region (Fig. 4). For easy quantification of the G-protein signaling levels, signal-responsive transcription was evaluated by using a *GFP* reporter gene [21,22].

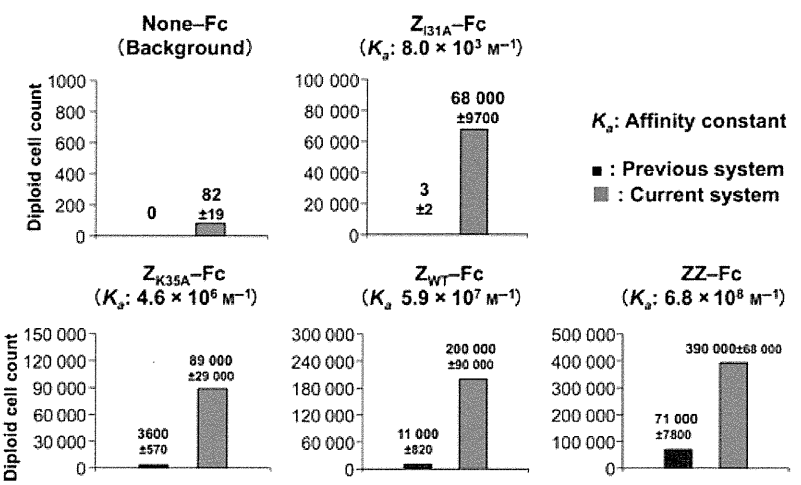

Fig. 2. Comparison of diploid formation in mating-based selection between the previous and current systems. Diploid formation selected on solid medium was investigated to test whether various ranges of protein–protein interactions can be screened. The numbers of generated diploid cells in an equivalent volume of 1 mL of cell suspension, with $D_{600\ nm}$ set at 1.0 (corresponding to $\sim 2 \times 10^7$ cells), are displayed. Standard deviations of three independent experiments are presented.

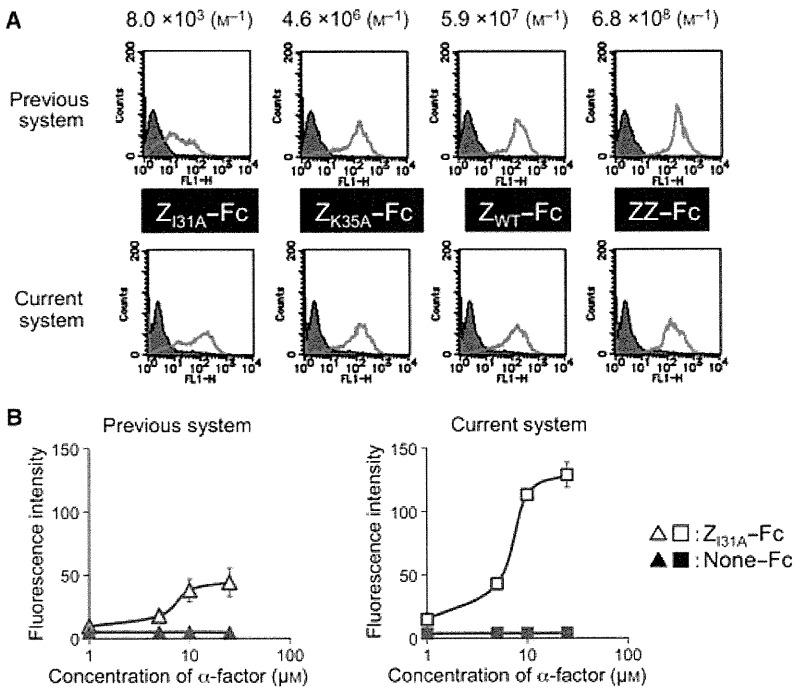

Fig. 3. Comparison of the G-protein signal levels between the previous and current systems by use of a GFP transcription assay. (A) Flow cytometric fluorescence analyses for comparison of the G-protein signal levels. Fluorescence intensity (FL-1H) of yeast strains containing different counterparts of the Fc region measured in the previous and current systems, respectively (open histograms). Closed histogram plots indicate yeast strains possessing None–Fc as the counterpart of the Fc region. To investigate the signal levels, 5 μM α-factor was used for each strain. The histogram plots show the analytical data for 10 000 cells. (B) Concentration–response curves for the α-factor in the previous system, indicated by triangle symbols, and in the current system, indicated by square symbols. Open symbols indicate concentration–response curves of yeast strains possessing the Z_{I31A}–Fc interaction, and closed symbols indicate those of the yeast strains possessing None–Fc as the counterpart of the Fc region. The fluorescence intensity indicates the average value in the 10 000 cells analyzed. Standard deviations of three independent experiments are presented.

Z_{EGFR} is a variant of the Z-domain with its binding target genetically altered from the Fc region to the epidermal growth factor receptor (EGFR) [23], and HXT1p is an endogenous hexose transporter that serves as a model membrane-localized protein [24]. These counterparts should have no affinity for the Fc region. As shown in Fig. 4, the interaction between Z_{I31A} and Fc produced GFP fluorescence in response to G-protein signaling (Z_{I31A}–Fc). However, the combination of Z_{EGFR} or HXT1p with Fc (Z_{EGFR}–Fc or Hxt1p–Fc) exhibited almost equivalent fluorescence as Fc expressed alone without the counterpart (None–Fc). These results demonstrate that the current system specifically detects protein–protein interactions.

Optimization of the screening procedure to exclude false-positive clones

Despite the successful selection of transient interactions, we observed scarce but detectable formation of diploid cells in the control strain without interacting protein pairs (Fig. 2; None–Fc; 82 diploid cell counts generated in an equivalent volume of 1 mL of cell suspension, with $D_{600\ nm}$ set at 1.0). This background signal might be attributable to the formation of false-positive clones, and be a serious problem for library screening. To ensure that our method screens only transient interactions, we tried to exclude the background signal by modifying the cultivation conditions with the mating partners (Fig. 5).

Our highly sensitive amplification system probably triggered the formation of background diploid cells, owing to the leaky expression of intact Gγ in response to the extremely low level of basal signaling. Hence, we measured the generated diploid cells at the early stage of cultivation in the mating process (Fig. 5A). After 3 h of cultivation (unmodified condition), ~ 100 diploid cells were generated as a background signal (FG0; None–Fc) in an equivalent volume of 1 mL of cell suspension ($D_{600\ nm}$ = 1.0). On the other hand,

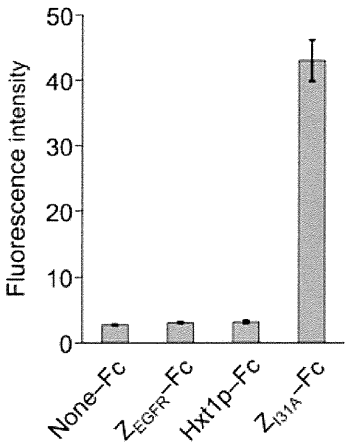

Fig. 4. Transcription activities that reflect G-protein signal levels triggered by the transient interaction between Z_{I31A} and Fc. GFP reporter expression for detecting protein–protein interactions was stimulated by addition of 5 μM α-factor to YPD medium. In addition to None–Fc, Z_{EGFR} (binder to EGFR) and Hxt1p (hexose transporter), which have no relationship with the Fc region, were utilized as negative controls (counterpart of the Fc region) to confirm the specific detection of interacting protein pairs in the current method. Z_{EGFR} and Z_{I31A} were modified to localize at the inner leaflet of the membrane by addition of the lipidation motif. Standard deviations of three independent experiments are presented.

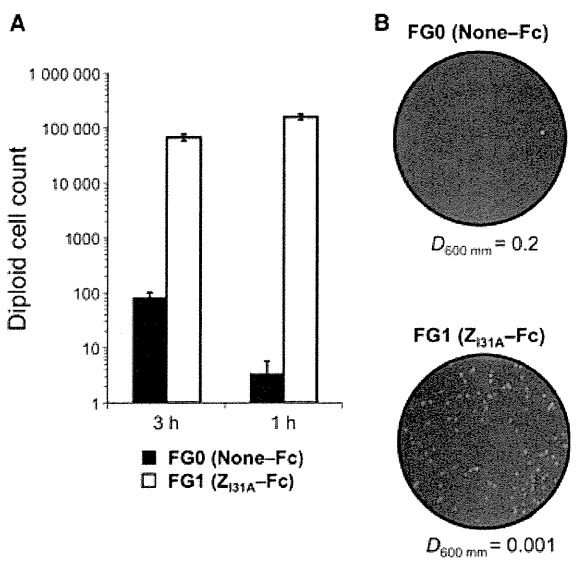

Fig. 5. Diploid cell formation in an optimized screening procedure to exclude false-positive clones. (A) The number of the generated diploid cells in an equivalent volume of 1 mL of cell suspension, with $D_{600\ nm}$ set at 1.0 (corresponding to $\sim 2 \times 10^7$ cells), on diploid selection solid medium. Yeast mating was performed in YPD medium at the indicated cultivation time. Standard deviations of three independent experiments are presented. (B) Direct images of diploid cell formation on selective solid medium after 1 h of mating. Cell suspensions were spread at the indicated cell densities (1 mL).

reducing the cultivation time to 1 h (modified condition) significantly decreased the formation of background diploid cells to fewer than five in the same equivalent volume. The number of diploid cells generated in response to the transient Z_{I31A}–Fc interaction (FG1) was almost the same as that in the unmodified condition.

Figure 5B shows direct images of the generation of diploid cells on selective solid medium after 1 h of cultivation. As compared with FG0 (None–Fc) spread with $D_{600\ nm}$ set at 0.2, FG1 (Z_{I31A}–Fc) produced a great number of diploid cells, although they were spread at much lower density ($D_{600\ nm}$ = 0.001). These results clearly demonstrate that our method permitted the isolation of the weak and transient Z_{I31A}–Fc interaction by mating-based selection, indicating that other weak and transient interactions should also be screened at high frequency in our system.

Model screening to compare the previous system and the current signal amplification system

Finally, to clarify the capabilities of the current Gγ recruitment system incorporating a signal amplification circuit, model screenings were carried out. The combination of Z_{I31A} and Fc was selected as a model of the transient interacting protein pair. For comparison, two artificial libraries were prepared. As in the previous system, one contained a minor amount of target strain (BFG2Z18-I31A; Z_{I31A}–Fc) and an excess amount of nontarget strain (BFG2118; None–Fc). As in the current system, the other contained a minor amount of signal-amplifiable target strain (FG1; Z_{I31A}–Fc) and an excess amount of signal-amplifiable nontarget strain (FG0; None–Fc). Several mixing ratios were used, as shown in Table 2. The final ratios of target cells were decided by checking the insertions of Z_{I31A} in diagnostic PCR of 10 colonies generated on selective solid medium. Whereas the previous system could never isolate the target cells even from the library with 1% of the initial target population, the current signal amplification system displayed successful isolations of the target cells, with 100% of final ratio of target cells from the model library with 1% and 0.1% frequency of target cells (Table 2). These results demonstrate the superiority of the Gγ recruitment system incorporating a novel signal amplification circuit, which can isolate the candidates for the transient interactions from genetic libraries, although further improvements in the screening efficiencies are required to accommodate larger-scale libraries. In addition, as our recruitment system leads to a false-positive readout resulting from expression of membrane proteins or

Table 2. Model screening of target cells expressing Z_{I31A} and Fc as a transient interacting protein pair.

Amplification system consisting of FG1 and excess FG0				Previous system consisting of BFG2Z18-I31A and excess BFG2118			
Initial ratio of target cells (%)	Initial cell number[a]	Generated diploid cell number	Final ratio of target cells[b]	Initial ratio of target cells (%)	Initial cell number	Generated diploid cell number	Final ratio of target cells (%)
1	4 000 000	65	100	1	4 000 000	0	–
0.1	10 000 000[c]	19	100	0.1	4 000 000	0	–
0.01	4 000 000	0	–	0.01	4 000 000	0	–

[a] Initial cell number used for screening was calculated from the value of $D_{600\ nm}$. [b] Final ratio of target cells was determined by checking the colony number retaining the target Z_{I31A} gene among 10 colonies. [c] The number of initial cells was set to generate > 10 colonies of diploid cells for determination of final ratio of the target cells, if available.

membrane-associated proteins from the cDNA library, a creative strategy to exclude the false positives will be needed for the practical use of our approach.

In conclusion, we have established a powerful approach to screen weak and transient protein–protein interactions by incorporating a novel signal amplification circuit with intact Gγ as an artificial signal amplifier on the basis of our previous Gγ recruitment system. Because our system allows mating-based growth selection, the screening procedure is extremely simple and does not require expensive instruments. We successfully demonstrated the utility of the current system as compared with our previous system, suggesting that it can be reliably used to screen for transient interactions from large-scale genetic libraries.

Materials and methods

Strains and media

The genotypes of *Saccharomyces cerevisiae* used in this study are outlined in Table 1. Details of plasmid construction and yeast transformation are presented in Doc. S1. The nucleotides for construction of plasmids and yeast strains are listed in Table S1. YPD medium contained 1% yeast extract, 2% peptone, and 2% glucose. SD medium contained 0.67% yeast nitrogen base without amino acids (BD-Diagnostic Systems, Sparks, MD, USA) and 2% glucose; 2% agar was added for solid media.

Transcription assay with *EGFP* fluorescent reporter gene

The *FIG1–EGFP* fusion gene was used as a fluorescent reporter gene [19,20]. Stimulation of the signaling mediated by protein–protein interactions was started by adding 5 μM α-factor to YPD medium. The cells were incubated at 30 °C for 6 h, and the GFP fluorescence intensities of the cells were then measured on a FACSCalibur equipped with a 488-nm air-cooled argon laser (BD Biosciences, San Jose, CA, USA).

Diploid growth selection

Quantification of mating abilities was performed by colony counting as follows. Each engineered yeast strain was cultivated in 1 mL of YPD medium with the mating partner BY4742 (Table 1) at 30 °C for 3 or 1 h, with the initial $D_{600\ nm}$ of each haploid cell set at 0.1. After cultivation, yeast cells were harvested, washed, and resuspended in distilled water. Cell suspensions were spread on SD solid medium without methionine and lysine but containing 20 mg·L^{-1} histidine, 30 mg·L^{-1} leucine, and 20 mg·L^{-1} uracil (SD – Met,Lys plate) with the appropriate dilution factor for each strain. After incubation at 30 °C for 2 days, the measured colony number was multiplied by each dilution factor to estimate the number of diploid cells generated in an equivalent volume of 1 mL of cell suspension, with $D_{600\ nm}$ set at 1.0.

Screening of target cells from model libraries

Model libraries were prepared by mixing the target cells (FG1 or BFG2Z18-I31A) with control cells (FG0 or BFG2118) in the initial ratios shown in Table 2. These libraries were cultivated in 1 mL of YPD medium with mating partner BY4742 at 30 °C for 1 h, with the initial $D_{600\ nm}$ of each haploid cell set at 0.1. After cultivation, yeast cells were harvested, washed, applied to SD – Met,Lys plates, and incubated at 30 °C for 2 days. Ten colonies were picked and separately grown in YPD medium overnight. The genomes were extracted, and the target Z_{I31A} gene was amplified by PCR with primers 5′-AAATA TAAAACGCTAGCGTCGACATGGCGC-3′ and 5′-AGC GTAAAGGATGGGGAAAG-3′. The final ratio of target cells was determined by counting the number of colonies retaining the target genes.

Acknowledgements

This work was supported by a Research Fellowship for Young Scientists from the Japan Society for the Promotion of Science, and in part by Special

Coordination Funds for Promoting Science and Technology, Creation of Innovation Centers for Advanced Interdisciplinary Research Areas (Innovative Bioproduction Kobe), MEXT, Japan. We are grateful to F. Matsuda, Organization of Advanced Science and Technology, Kobe University, for valuable discussion.

References

1 Perkins JR, Diboun I, Dessailly BH, Lees JG & Orengo C (2010) Transient protein–protein interactions: structural, functional, and network properties. *Structure* **18**, 1233–1243.
2 Fields S & Song O (1989) A novel genetic system to detect protein–protein interactions. *Nature* **340**, 245–246.
3 Aronheim A, Engelberg D, Li N, al-Alawi N, Schlessinger J & Karin M (1994) Membrane targeting of the nucleotide exchange factor Sos is sufficient for activating the Ras signaling pathway. *Cell* **78**, 949–961.
4 Johnsson N & Varshavsky A (1994) Split ubiquitin as a sensor of protein interactions *in vivo*. *Proc Natl Acad Sci USA* **91**, 10340–10344.
5 Ehrhard KN, Jacoby JJ, Fu XY, Jahn R & Dohlman HG (2000) Use of G-protein fusions to monitor integral membrane protein–protein interactions in yeast. *Nat Biotechnol* **18**, 1075–1079.
6 Urech DM, Lichtlen P & Barberis A (2003) Cell growth selection system to detect extracellular and transmembrane protein interactions. *Biochim Biophys Acta* **1622**, 117–127.
7 Gietz RD, Triggs-Raine B, Robbins A, Graham KC & Woods RA (1997) Identification of proteins that interact with a protein of interest: applications of the yeast two-hybrid system. *Mol Cell Biochem* **172**, 67–79.
8 Takesako K, Ikai K, Haruna F, Endo M, Shimanaka K, Sono E, Nakamura T, Kato I & Yamaguchi H (1991) Aureobasidins, new antifungal antibiotics. Taxonomy, fermentation, isolation, and properties. *J Antibiot* **44**, 919–924.
9 Zheng D, Cho YY, Lau AT, Zhang J, Ma WY, Bode AM & Dong Z (2008) Cyclin-dependent kinase 3-mediated activating transcription factor 1 phosphorylation enhances cell transformation. *Cancer Res* **68**, 7650–7660.
10 Chen J, Zhou J, Bae W, Sanders CK, Nolan JP & Cai H (2008) A yEGFP-based reporter system for high-throughput yeast two-hybrid assay by flow cytometry. *Cytometry A* **73**, 312–320.
11 Fukuda N, Ishii J, Tanaka T, Fukuda H & Kondo A (2009) Construction of a novel detection system for protein–protein interactions using yeast G-protein signaling. *FEBS J* **276**, 2636–2644.
12 Fukuda N, Ishii J, Tanaka T & Kondo A (2010) The competitor-introduced Gγ recruitment system, a new approach for screening affinity-enhanced proteins. *FEBS J* **277**, 1704–1712.
13 Ishii J, Fukuda N, Tanaka T, Ogino C & Kondo A (2010) Protein–protein interactions and selection: yeast-based approaches that exploit guanine nucleotide-binding protein signaling. *FEBS J* **277**, 1982–1995.
14 Manahan CL, Patnana M, Blumer KJ & Linder ME (2000) Dual lipid modification motifs in Gα and Gγ subunits are required for full activity of the pheromone response pathway in *Saccharomyces cerevisiae*. *Mol Biol Cell* **18**, 957–968.
15 Kronvall G & Williams RC Jr (1969) Differences in anti-protein A activity among IgG subgroups. *J Immunol* **103**, 828–833.
16 Nilsson B, Moks T, Jansson B, Abrahmsén L, Elmblad A, Holmgren E, Henrichson C, Jones TA & Uhlén M (1987) A synthetic IgG-binding domain based on staphylococcal protein A. *Protein Eng* **1**, 107–113.
17 Jendeberg L, Persson B, Andersson R, Karlsson R, Uhlén M & Nilsson B (1995) Kinetic analysis of the interaction between protein A domain variants and human Fc using plasmon resonance detection. *J Mol Recognit* **8**, 270–278.
18 Brachmann CB, Davies A, Cost GJ, Caputo E, Li J, Hieter P & Boeke JD (1998) Designer deletion strains derived from *Saccharomyces cerevisiae* S288C: a useful set of strains and plasmids for PCR-mediated gene disruption and other applications. *Yeast* **14**, 115–132.
19 Iguchi Y, Ishii J, Nakayama H, Ishikura A, Izawa K, Tanaka T, Ogino C & Kondo A (2010) Control of signalling properties of human somatostatin receptor subtype-5 by additional signal sequences on its amino-terminus in yeast. *J Biochem* **147**, 875–884.
20 Togawa S, Ishii J, Ishikura A, Tanaka T, Ogino C & Kondo A (2010) Importance of asparagine residues at positions 13 and 26 on the amino-terminal domain of human somatostatin receptor subtype-5 in signalling. *J Biochem* **147**, 867–873.
21 Ishii J, Tanaka T, Matsumura S, Tatematsu K, Kuroda S, Ogino C, Fukuda H & Kondo A (2008) Yeast-based fluorescence reporter assay of G protein-coupled receptor signalling for flow cytometric screening: *FAR1*-disruption recovers loss of episomal plasmid caused by signalling in yeast. *J Biochem* **143**, 667–674.
22 Ishii J, Izawa K, Matsumura S, Wakamura K, Tanino T, Tanaka T, Ogino C, Fukuda H & Kondo A (2009) A simple and immediate method for simultaneously evaluating expression level and plasmid maintenance in yeast. *J Biochem* **145**, 701–708.
23 Friedman M, Nordberg E, Höidén-Guthenberg I, Brismar H, Adams GP, Nilsson FY, Carlsson J & Ståhl S (2007) Phage display selection of Affibody molecules with specific binding to the extracellular domain of the epidermal growth factor receptor. *Protein Eng Des Sel* **20**, 189–199.

24 Lewis DA & Bisson LF (1991) The HXT1 gene product of *Saccharomyces cerevisiae* is a new member of the family of hexose transporters. *Mol Cell Biol* **11**, 3804–3813.

Supporting information

The following supplementary material is available:
Doc. S1. Supporting information for Materials and methods; details of the construction of strains and plasmids are given.

Table S1. List of oligonucleotides for construction of plasmids and yeast strains.

This supplementary material can be found in the online version of this article.

Please note: As a service to our authors and readers, this journal provides supporting information supplied by the authors. Such materials are peer-reviewed and may be re-organized for online delivery, but are not copy-edited or typeset. Technical support issues arising from supporting information (other than missing files) should be addressed to the authors.

Analytical Biochemistry 417 (2011) 182–187

Contents lists available at ScienceDirect

Analytical Biochemistry

journal homepage: www.elsevier.com/locate/yabio

Amplification of agonist stimulation of human G-protein-coupled receptor signaling in yeast

Nobuo Fukuda [a], Jun Ishii [b], Misato Kaishima [a], Akihiko Kondo [a,*]

[a] Department of Chemical Science and Engineering, Graduate School of Engineering, Kobe University, Nada-ku, Kobe 657-8501, Japan
[b] Organization of Advanced Science and Technology, Kobe University, Nada-ku, Kobe 657-8501, Japan

ARTICLE INFO

Article history:
Received 11 March 2011
Received in revised form 27 May 2011
Accepted 6 June 2011
Available online 13 June 2011

Keywords:
Yeast
GPCR
G-protein signaling
Gβ subunit
Feedback signal activation

ABSTRACT

G-protein-coupled receptors (GPCRs) are considered as important targets for drug discovery. The yeast *Saccharomyces cerevisiae* is an attractive host for high-throughput screening of agonistic ligands for human GPCRs because it can simplify the complicated signaling pathways that are present in mammalian cell lines. Unfortunately, many human GPCRs induce only partial signal activation in yeast cells depending on their coupling efficiency with yeast G-proteins. This problem often results in unsatisfactory detection sensitivity, thereby resulting in a limitation to yeast-based detection systems. Here we introduce a new highly sensitive detection method that provides robust agonist detection of human GPCRs. Our strategy is designed to invoke feedback activation of signals within yeast G-protein signaling pathways. Briefly, agonist stimulation of human GPCRs triggers expression of an artificial signal activator that amplifies signaling. We chose human somatostatin receptor subtype 5 (hSSTR5) as a model of a human GPCR. Investigation of the response of hSSTR5-expressing yeast to various concentrations of somatostatin demonstrated that feedback activation of the signal can successfully improve the detection limit and the maximum level of signaling. This novel approach will enhance the usefulness of yeast-based screening of agonistic ligands for a variety of human GPCRs.

G-protein-coupled receptors (GPCRs)[1] constitute the largest family of transmembrane proteins and play an important part in signal transduction by converting extracellular stimuli into intracellular signals. Currently, more than 30% of marketed medicines act on GPCRs, which are still considered as attractive targets for new medicines [1]. To develop new medicines, it is necessary to evaluate a lot of candidates due to the low frequency of discovery of lead compounds. Therefore, high-throughput screening (HTS) of active compounds has become an integral technology in pharmaceutical laboratories [2].

The budding yeast *Saccharomyces cerevisiae* is an attractive host cell system for identification of agonistic ligands that can modulate the functions of human GPCRs because the mechanisms of G-protein signaling are highly conserved among a diverse range of eukaryotes from yeast to mammals. The yeast system, which is composed of an uncompetitive and monopolistic G-protein signaling pathway (the pheromone signaling pathway) [3], is more simple than the complicated G-protein signaling that occurs in mammalian cell lines. It has also been reported that a variety of human GPCRs can successfully activate the yeast signaling pathway when expressed in yeast cells. These receptors respond to binding of their agonists and transmit signals via coupling with the endogenous yeast G-protein, which is a heterotrimer consisting of Gα, Gβ, and Gγ subunits [4]. Whereas a heterotrimeric Gαβγ complex is formed in the unstimulated state (without agonistic ligand), binding of agonist to the receptor induces dissociation of the heterotrimeric G-protein into monomeric Gα and a Gβγ complex, which is accompanied by the exchange of GDP for GTP on the Gα subunit (Fig. 1A). In yeast, the dissociated Gβγ complex activates intracellular effector proteins that stimulate the mitogen-activated protein kinase (MAPK) cascade, resulting in changes in cell behavior (Fig. 1A).

Because cellular responses to MAPK activation, including changes in gene transcription, can be used to detect GPCR agonist-induced signaling, several reporter gene assays have been adopted to assay the signaling stimulated by GPCR agonists in yeast systems (Fig. 1A). Although the *HIS3* and *lacZ* genes [5,6] are conventional reporter genes that are used for auxotrophic screening and colorimetric evaluation, respectively, it was recently reported that a *GFP* fluorescent reporter gene can be used for quantitative HTS using flow cytometry [7–9]. One problem with using

* Corresponding author. Fax: +81 78 803 6196.
E-mail address: akondo@kobe-u.ac.jp (A. Kondo).

[1] *Abbreviations used:* GPCR, G-protein-coupled receptor; HTS, high-throughput screening; MAPK, mitogen-activated protein kinase; hSSTR5, human somatostatin receptor subtype 5; PCR, polymerase chain reaction; EGFP, enhanced green fluorescent protein; SST, somatostatin.

0003-2697/$ - see front matter © 2011 Elsevier Inc. All rights reserved.
doi:10.1016/j.ab.2011.06.006

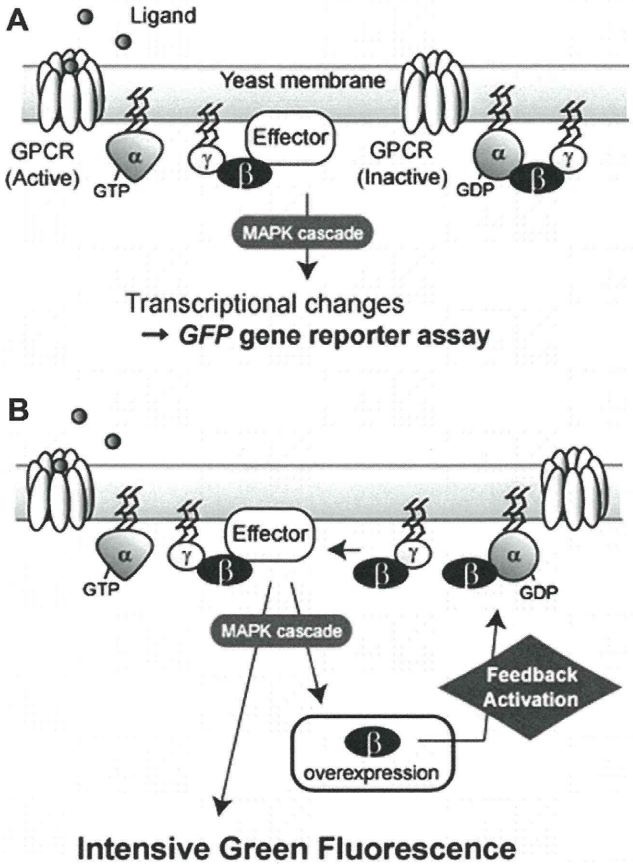

Fig.1. (A) Schematic outline of the strategy of *feedback signal activation* system commonly used to analyze agonist stimulation of GPCRs using the yeast pheromone signaling pathway. Agonistic ligand binding to the GPCR leads to activation of heterotrimeric G-proteins composed of Gpa1 (Gα), Ste4 (Gβ), and Ste18 (Gγ). The activated G-proteins subsequently dissociate into Gα and a Gβγ dimer. The Gβγ dimer induces activation of the MAPK cascade, resulting in expression of a *GFP* reporter gene. (B) Feedback signal activation approach for robust and highly sensitive detection of GPCR agonists. Ligand stimulation induces the expression of both *GFP* and *STE4* (Gβ) genes. This Gβ that is overexpressed in a signal-responsive manner competes with endogenous Gβ present in the Gαβγ heterotrimer for Gα binding. Such competition releases a free Gβγ complex that can amplify the weak signal caused by partial coupling between the heterologous GPCR and endogenous yeast G-protein. The resulting intense green fluorescence improves the sensitivity of heterologous GPCR signal detection.

yeast systems for analysis of human GPCR signaling is that the level of the signals transmitted from human GPCRs is commonly lower than that from the endogenous yeast GPCR due to inefficient coupling between the yeast G-protein and the human GPCR [10]. Thus, high signal-to-noise ratio in reporter gene assays is a critical factor in order to achieve powerful and reliable screening of human GPCR agonists. Therefore, a highly sensitive system that can detect reporter genes in yeast even in response to weak signals would be beneficial for screening of human GPCR agonists.

Here we describe a novel strategy to improve the sensitivity of detection of agonist-dependent signaling of a human GPCR that is expressed on a yeast cell surface. Because this strategy involves signal-induced expression of a gene encoding an activator (Gβ subunit) of the effector protein that is the output of yeast G-protein signaling, induction of this gene is expected to result in persistent activation of the MAPK cascade after signal initiation (Fig. 1B). Thus, agonist addition switches on "feedback signal activation" of yeast G-protein signaling. In the current study, we show the feasibility of this approach and its potency for the detection of human GPCR agonists.

Materials and methods

Strains, plasmids, and media

The genotypes of the *S. cerevisiae* strains and plasmids used in this study are outlined in Table 1. Yeast cells were grown in YPD medium containing 1% (w/v) yeast extract, 2% peptone, and 2% glucose, in SD medium containing 0.67% yeast nitrogen base without amino acids (Becton Dickinson, Franklin Lakes, NJ, USA) and 2% glucose, or in SDM71 medium (SD medium adjusted to pH 7.1 with 200 mM Mopso buffer) [11].

Construction of plasmids

To express the *STE4* gene (encoding Gβ) under the control of the pheromone-responsive *FIG1* promoter [11–15], the *STE4* gene was inserted into a plasmid that integrated into the yeast chromosome at a position upstream of the *HOP2* gene (P_{HOP2}:*HOP2* promoter region). Plasmid construction was as follows. The *STE4* gene was amplified from BY4741 [16] genomic DNA using the primers 5′-aaaaGTCGACatggactacaaggatgacgatgacaaggcagcacatcagatggactcgataacgt-3′ and 5′-aaaaGGATCCctattgataacctggagacc-3′ (restriction enzyme sites are in uppercase letters) and was inserted into the *Sal*I–*Bam*HI sites of pLMFIG-STE18-H [17], yielding the plasmid pLMFIG-STE4-H.

The plasmid used for expression of the human somatostatin receptor subtype 5 (hSSTR5) was constructed as follows. A DNA fragment encoding the *hSSTR5* gene was amplified from pGK-SSTR5-HA [11] using the primers 5′-ccccGTCGACatggagcccctgttcc cagc-3′ and 5′-ccccGAATTCtcacagcttgctggtctgca-3′ (restriction enzyme sites are in uppercase letters) and was inserted into the *Sal*I–*Eco*RI sites between the *PGK1* promoter (P_{PGK1}) and the *PGK1* terminator (T_{PGK1}) on pGK423 [18], yielding the plasmid pHM-SSTR5 (Table 1).

Construction of yeast strains

Each DNA fragment was introduced into yeast cells using the lithium acetate method [19]. The DNA fragments containing *LEU2*-P_{FIG1}-*STE4*-T_{PGK1}-P_{HOP2} were amplified from pLMFIG-STE4-H using the primers 5′-atacaattaattgacatcagcagacagcaaatgcacttgatatacgcagctcgactacgtcgtaaggccg-3′ (corresponding to 50 nt of the region directly upstream of P_{HOP2}) and 5′-atctttcaaatagagcctgg-3′ and were used to transform MC-F1 [17]. The transformants were

Table 1
List of yeast strains and plasmids used in this study.

Strain or plasmid	Description	Reference source
Yeast strains		
BY4741	*MAT***a** *his3Δ1 ura3Δ0 leu2Δ0 met15Δ0*	[16]
MC-F1	BY4741 *fig1*::*FIG1-EGFP*	[17]
MC-F1B	MC-F1 P_{HOP2}::*LEU2*-P_{FIG1}-*STE4*	This study
IMFD-70	BY4741 *sst2Δ*::*AUR1-C ste2Δ*::*LEU2 fig1Δ*::*EGFP his3Δ*::P_{FIG1}-*EGFP far1Δ*	[11]
IMFD-70B	IMFD-70 P_{HOP2}::*URA3*-P_{FIG1}-*STE4*	This study
Plasmids		
pGK411	Yeast expression vector containing *PGK1* promoter, *CEN/ARS* origin, and *MET15* marker	[21]
pGK411-STE2	*STE2* in pGK411	[21]
pGK423	Yeast expression vector containing *PGK1* promoter, 2μ origin, and *HIS3* marker	[18]
pHM-SSTR5	*hSSTR5* in pGK423	This study

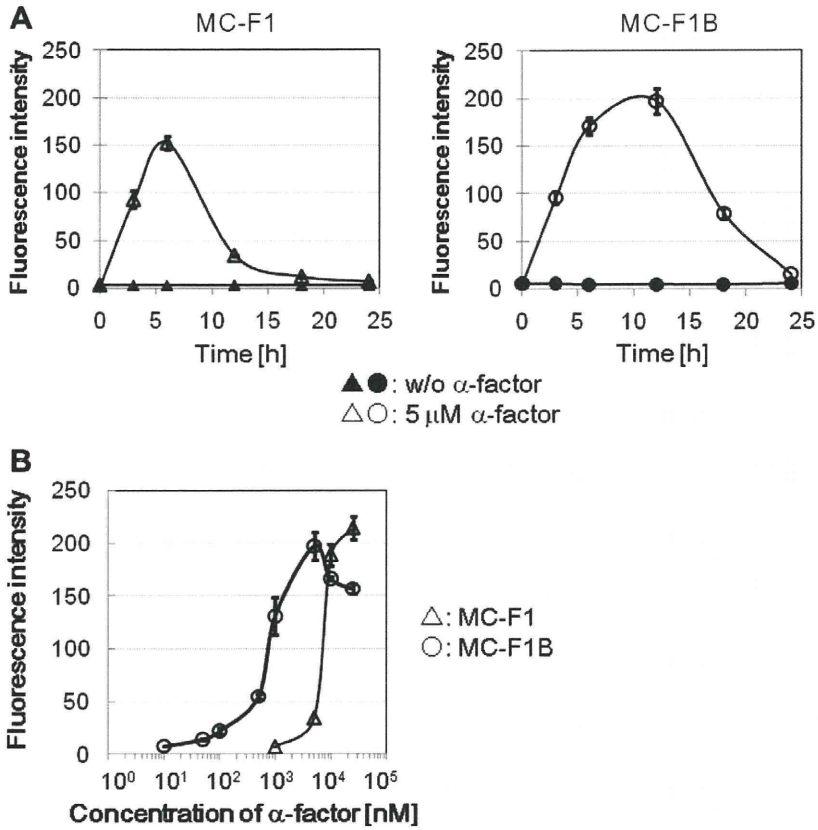

Fig.2. Fluorescence of a *GFP* reporter gene in response to agonist stimulation of the endogenous yeast Ste2 receptor in common and feedback activation strains. (A) Fluorescence of *GFP* reporter genes in the common activation yeast strain (MC-F1) and in the feedback signal activation strain (MC-F1B) with or without 5 μM α-factor stimulation. (B) Concentration–response curves of MC-F1 and MC-F1B to α-factor. The fluorescence intensities indicate the average values of 10,000 cells. The results are presented as means ± standard deviations of three independent experiments. w/o, without.

selected on SD solid medium without leucine but containing 20 mg/L uracil and histidine and 30 mg/L methionine (SD-Leu plate) to yield the MC-F1B strain (Table 1).

DNA fragments containing *URA3*-P_{FIG1}-*STE4*-T_{PGK1}-P_{HOP2} were constructed by overlap extension polymerase chain reaction (PCR) [20]. The *URA3*-containing fragment was amplified from pGK426 [18] using the primers 5′-cagacagcaaatgcac ttgatatacgcagcttcaatt-catcatttttttt-3′ (corresponding to 30 nt of the region directly upstream of P_{HOP2}) and 5′-gcgtttggttgatcattcaaggg taataactgatataa ttaaattgaagc-3′. The fragment containing P_{FIG1}-*STE4*-T_{PGK1}-P_{HOP2} was amplified from pLMFIG-STE4-H using the primers 5′-gcttcaatt-taattatatcagt tattacccttgaatgatcaaccaaacgccgatatagtc-3′ and 5′-atctttcaaatagagcctgg-3′. These two DNA fragments were ligated and used to transform IMFD-70 [11]. The transformants were selected on SD solid medium without uracil but containing 20 mg/L histidine and 30 mg/L leucine and methionine (SD-Ura plate) to yield the IMFD-70B strain (Table 1). The GPCR expression plasmids pGK411-Ste2 [21] and pHM-SSTR5 were used to transform both IMFD-70 and IMFD-70B strains.

Transcription assay using GFP fluorescent reporter gene

The Fig1p-EGFP (enhanced green fluorescent protein) fusion protein was used as a fluorescent reporter. The yeast cells were incubated at 30 °C, and their fluorescence intensities were then measured using a FACSCalibur equipped with a 488-nm air-cooled argon laser (Becton Dickinson). The data were analyzed using CELLQuest software (Becton Dickinson), and the average fluorescence intensity of 10,000 cells was defined as the geometric mean.

Fluorescence microscopic imaging

After incubation for 18 h at 30 °C, the yeast cells were washed and suspended in distilled water. The cell suspensions were observed using a BZ-9000 fluorescence microscope (Keyence, Osaka, Japan). Fluorescence images were acquired with a 510-nm band-pass filter for emission.

Results and discussion

General strategy

The aim of this study was to establish a sensitive and robust method for the detection of yeast G-protein signaling in order to enhance the usefulness of yeast-based systems for screening of agonistic ligands of human GPCRs. Our strategy was designed to trigger feedback activation of G-protein signaling through signal-induced expression of an artificial signal activator. The endogenous yeast Gβ subunit was selected as the signal activator because overexpression of Gβ constitutively activates the MAPK cascade through effector proteins even in the absence of agonists [22–24]. As shown in Fig. 1B, overexpression of a signal-responsive Gβ subunit is expected to result in the generation of free Gβγ complexes by competing with the endogenous γ-associated β subunit for binding to the α subunit. This competition would result in the release of free βγ dimers, which could then amplify the weak signal caused by partial coupling between the heterologous human GPCR and the endogenous yeast G-protein.

Based on the above theory, we constructed a recombinant yeast strain in which overexpression of the *STE4* gene that encodes the

yeast Gβ subunit can be induced by the signal-responsive *FIG1* promoter [11–15]. Initiation of G-protein signaling in this yeast by agonist stimulation was expected to lead to a feedback activation of G-protein signaling through this overexpressed Gβ subunit (Fig. 1B). We termed this strategy *feedback signal activation.* The endogenous yeast GPCR, the Ste2 receptor that interacts with endogenous yeast G-proteins, was first used to test our hypothesis that overexpression of a signal-responsive Gβ subunit would invoke feedback signal activation. Subsequently, the hSSTR5 was used to verify that such feedback signal activation allows highly sensitive and robust detection of agonists of human GPCRs on yeast cell surfaces.

Demonstration of feedback signal activation using the endogenous yeast GPCR

To validate our hypothesis, we constructed the yeast strain, MC-F1B, in which overexpression of the *STE4* gene is under the control of the signal-responsive *FIG1* promoter (Table 1). MC-F1B is derived from the MC-F1 yeast strain in which the chromosomal gene that encodes the endogenous yeast Ste2 receptor is intact and in which a *GFP* reporter gene is integrated at the *FIG1* locus to detect signaling in response to agonist stimulation (Table 1) [17].

The fluorescence of the *GFP* reporter gene in these two yeast strains was quantitatively evaluated during cultivation with 5 μM α-factor (an Ste2p agonist) in YPD medium. As shown in Fig. 2A, the modified strain (MC-F1B) displayed almost the same fluorescence intensity as the parental strain (MC-F1) over the first 6 h of cultivation. Subsequently, although the fluorescence of MC-F1 dramatically decreased due to inactivation of Ste2p signaling following receptor desensitization, the fluorescence of the MC-F1B strain was prolonged and GFP fluorescence was augmented for up to 12 h of cultivation. This result indicated that induction of the integrated *STE4* gene amplified signaling induced by Ste2p and that the overexpressed Gβ protein successfully invoked feedback activation of yeast G-protein signaling.

We further investigated the α-factor concentration dependency of this signaling to determine the ligand sensitivity of these strains. Data obtained after 12 h of cultivation were used to construct concentration–response curves (Fig. 2B). In the case of MC-F1, fluorescence intensity started to strongly increase at a concentration of approximately 5 μM α-factor and reached a maximum level at a concentration of 10–50 μM α-factor in a manner similar to that reported previously [25]. The half-maximal effective concentration (EC_{50}) value was 7 μM. In contrast, the fluorescence intensity of MC-F1B began to increase at a concentration of approximately 500 nM α-factor and reached its maximum at a concentration of 5 μM α-factor. The EC_{50} value was 800 nM. A similar difference in dose responses was also confirmed even when comparing the MC-F1 and MC-F1B at each optimal cultivation time (MC-F1 at 6 h and MC-F1B at 12 h) (see Supplementary Fig. S1 in supplementary material).

Although these results demonstrated that our feedback signal activation strategy is viable and can expand the detection limit of GPCR signaling to a lower concentration of agonistic ligand α-factor, the maximum intensity of GFP fluorescence at higher concentrations of α-factor did not increase (Fig. 2B). These data likely reflect the fact that the endogenous Ste2 receptor can couple efficiently with its intracellular cognate yeast G-protein in response to a native agonist, the α-factor.

Expression of the yeast Ste2 receptor using an episomal plasmid in a gene-deleted strain

Most heterologous GPCR assays in yeast systems are performed in several types of gene deletion mutants. Thus, the *SST2*-deleted strain confers hypersensitivity toward agonistic ligands, and the *FAR1*-deficient strain allows cell growth and plasmid recovery even in signal-activated states [21]. Moreover, the endogenous yeast *STE2* gene is often deleted to avoid competition of Ste2 receptor expression on the cell surface with that of human GPCRs [21]. Target GPCRs are commonly expressed from episomal plasmids in such yeast strains.

Unfortunately, however, signaling levels observed using episomal plasmid expression systems are frequently lower than those observed using chromosomal expression systems. One possible explanation of this difference might be due to the different cultivation conditions with YPD and SD media. To examine whether feedback signal activation can occur when using GPCRs expressed from episomal plasmids in strains with Ste2 and other deletions, we selected the IMFD-70 strain, which has triple deletion alleles (*sst2*Δ, *far1*Δ, and *ste2*Δ) and *GFP* reporter genes, as the parental yeast strain (Table 1) [11]. We then integrated the artificial signal activator *STE4* gene into the IMFD-70 chromosome, yielding the IMFD-70B strain (Table 1). To model episomal expression systems, the single-copy autonomous replicating plasmid for expression of the endogenous yeast Ste2 receptor (pGK411-STE2) [21] was introduced into both IMFD-70 and IMFD-70B strains.

The fluorescence of the *GFP* reporter gene of these two strains was then quantitatively evaluated during cultivation with 50 nM α-factor in SD selection medium. As shown in Fig. 3A, IMFD-70B/Ste2p (the feedback activation strain) maintained GFP fluorescence for a longer time (up to 18 h) than IMFD-70/Ste2p (the common activation strain, up to 12 h). This increased time of GFP fluorescence in the *STE4* gene-overexpressing strain is similar to the results of strains with chromosomal *STE2* genes. However, unlike strains that express chromosomal Ste2p, IMFD-70B/Ste2p dis-

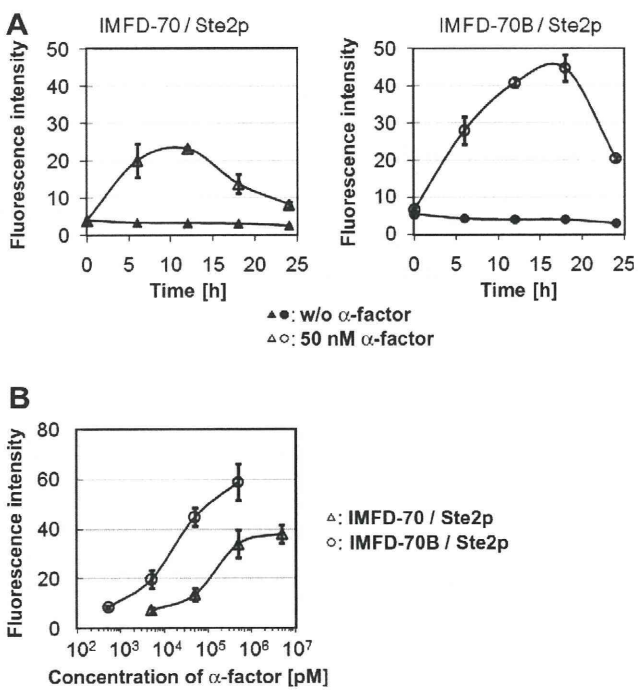

Fig.3. Fluorescence of a *GFP* reporter gene in response to agonist stimulation of common and feedback activation strains of yeast expressing the endogenous yeast Ste2 receptor gene from an episomal plasmid. (A) Fluorescence of the *GFP* reporter gene in the common activation strain (IMFD-70/Ste2p) and in the feedback signal activation strain (IMFD-70B/Ste2p) with or without 50 nM α-factor stimulation. (B) Concentration–response curves of IMFD-70/Ste2p and IMFD-70B/Ste2p to α-factor. The fluorescence intensities are the average values of 10,000 cells. The results are presented as means ± standard deviations of three independent experiments. w/o, without.